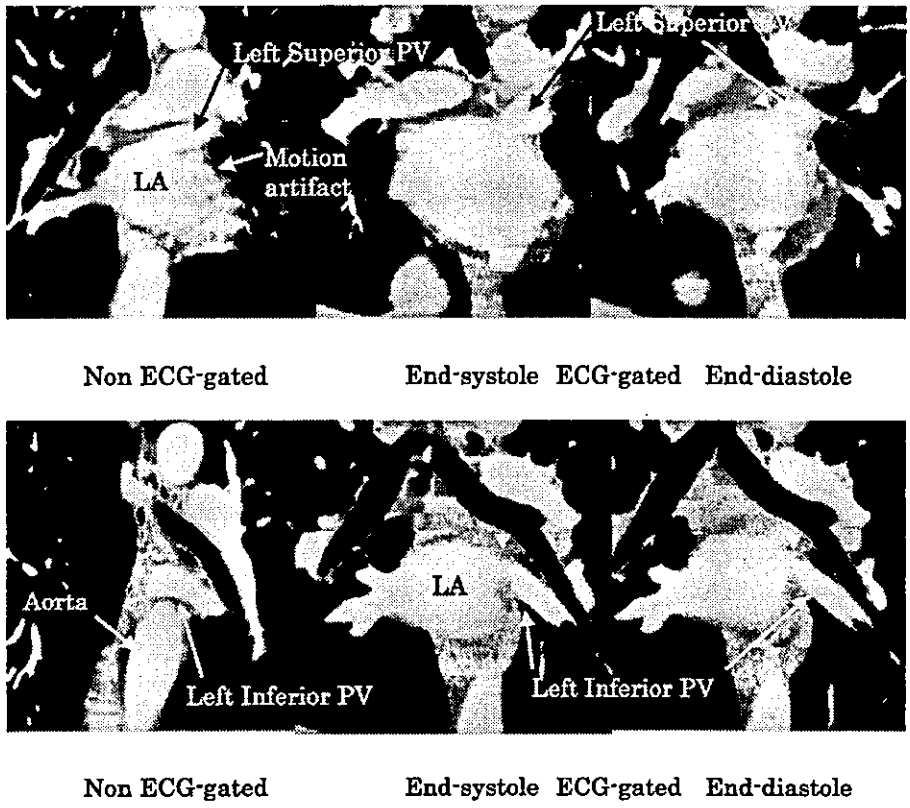

Fig. 2A,B. Anterior coronal views of the multiplanar reconstruction images of enhanced multislice computed tomography of nonelectrocardiogram (*ECG*)-gated acquisition images in a patient with another disease but a normal pulmonary vein (*PV*) and retrospective ECG-gated reconstruction images from end-systole and end-diastole in a patient after PV isolated catheter ablation. **A** Left superior PV level. **B** Left inferior PV level. There was a motion artifact in the non-ECG-gated images (in this case, in the left atrium (*LA*)) (*arrowheads*). In the ECG-gated reconstruction images, the resolution of the vessel to the through-plance was good an there was no motion artifact, allowing a clear image of the vessel lumen and the soft tissue around the vessel lumen (*arrowheads*) in the coronal view. In contrast to axial source images, the stenosis of the ostium of the left superior PV could be evaluated more clearly in end-systole than in end-diastole (the left inferior PV was almost the same in both cardiac phases in the coronal images)

the coronal images.) Therefore to evaluate the stenosis of the PV, it would be better to use volumetric images in several cardiac phases and several planes.

Figure 3 represents the three-dimensional volume rendering images using enhanced MSCT from end-systole in the same patient after PV isolation. The lumen of the vessel filled with the contrast material with high CT intensity and stenosis of the ostium of the left inferior PV could be observed (arrowhead).

Discussion

Generally, DSA only shows the vessel lumen filled with contrast material, while MSCT can evaluate hyperplasia of the soft tissue around the lumen of the PV, indicating a reaction to the PV isolation in addition to stenosis of the lumen of the PV. Therefore, MSCT may provide important indicators of this complication, or conversely, even the effectiveness of the PV isolation procedure. ECG-gated images, which have good resolution to the through-plane, may be evaluated in any plane desired, and might be superior to non-ECG-gated images with poor resolution and motion artifacts.

MRI is a noninvasive diagnostic method with excellent contrast resolution, which has no radiation exposure and eliminates the necessity of contrast material to evaluate the vessel lumen.[12,13] However, as the spatial resolution of MRI is currently less than that of MSCT, MSCT is more suitable for accurately detecting stenosis of the vessel. Furthermore, MRI requires a long acquisition time, while MSCT can achieve acquisition in a very short time and allow evaluation of the vessel from any direction desired. It is also difficult to use MRI to examine patients with claustrophobia.

The difference between the non-ECG-gated and ECG-gated reconstruction acquisition in MSCT is that the helical pitch must be set in retrospective ECG-gated reconstruction approximately one third of that with non-ECG-gated acquisition. This means that the total radiation dose of ECG-gated reconstruction is approximately three times as much as that of non-ECG-gated acquisition. But from the actual images presented in Figs. 1 and 2, we believe that ECG-gated reconstruction images may be justified in spite of the high radiation dose since we can evaluate the patient even in coronal views. Furthermore, using three-dimensional volume-rendering images, we can recognize the structure of the heart and great vessels, including the PV, with excellent clarity.

MSCT also can achieve prospective ECG-gated scanning. The total radiation dose of prospective ECG-gated scanning is much less than retrospective ECG-gated reconstruction scanning, so this method may be more advisable. However, this acquisition method cannot be used in patients with irregular heartbeats such as in Af. Furthermore, compared with retrospective ECG-gated reconstruction

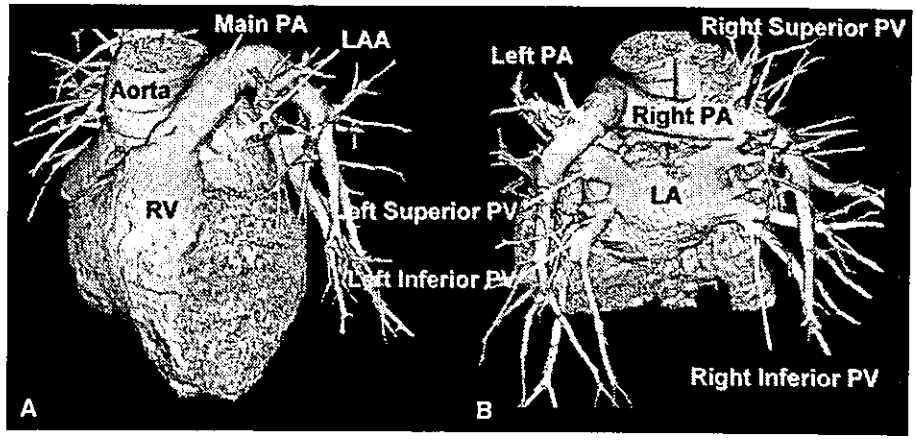

Fig. 3A,B. Three-dimensional volume-rendering images using enhanced multislice computed tomography (CT) from end-systole in a patient after pulmonary vein (*PV*) isolated catheter ablation. **A** Left anterior superior view. **B** Posterior view. Volume-rendering images represented the lumen of the vessel filled with the contrast material with high CT intensity. Stenosis of the ostium of the left inferior PV could be observed in the posterior view (*arrowhead*). *PA*, *RV*, *LA*, *LV*, and *LAA* indicate pulmonary artery, right ventricle, left atrium, left ventricle, and left atrial appendage, respectively

that can acquire volumetric data of any cardiac phase desired, this technique can only obtain volumetric images at one cardiac phase.

Conclusion

As PV isolation by catheter ablation to the ostium of the PV in subjects with paroxysmal Af is sometimes accompanied by complications, retrospective ECG-gated reconstruction acquisition using MSCT may assist in the evaluation of stenosis and hyperplasia of soft tissue around the lumen of the PV, and we feel that ECG-gated MSCT is the noninvasive diagnostic modality of choice. In the future, quantitative comparisons of the degree of stenosis of the lumen of the PV measured by DSA with that by MSCT will be necessary.

References

1. Oral H, Knight BP, Tada H, Ozaydin M, Chugh A, Hassan S, Scharf C, Lai SW, Greenstein R, Pelosi F Jr, Strickberger SA, Morady F (2002) Pulmonary vein isolation for paroxysmal and persistent atrial fibrillation. Circulation 105:1077–1081
2. Pappone C, Rosanio S, Oreto G, Tocchi M, Gugliotta F, Vicedomini G, Salvati A, Dicandia C, Mazzone P, Santinelli V, Gulletta S, Chierchia S (2000) Circumferential radiofrequency ablation of pulmonary vein ostia. A new anatomic approach for curing atrial fibrillation. Circulation 102:2619–2628
3. Pappone C, Oreto G, Rosanio S, Vicedomini G, Tocchi M, Gugliotta F, Salvati A, Dicandia C, Calabro MP, Mazzone P, Ficarra E, Di Gioia C, Guelletta S, Nardi S, Santinelli V, Benussi S, Alfieri O (2001) Atrial electroanatomic remodeling after circumferential radiofrequency pulmonary vein ablation: efficacy of an anatomic approach in a large cohort of patients with atrial fibrillation. Circulation 2001;104:2539–2544
4. Haïssaguerre M, Jaïs P, Shah DC, Garrigue S, Takahashi A, Lavergne T, Hocini M, Peng JT, Roudaut R, Clementy J (2000) Electrophysiological end point for catheter ablation of atrial fibrillation initiated from multiple pulmonary venous foci. Circulation 101:1409–1417
5. Chang KC, Lin YC, Chen JY, Chou HT, Hung JS (2001) Electrophysiological characteristics and radiofrequency ablation to focal atrial tachycardia originating from the superior vena cava. Jpn Circ J 65:1034–1040
6. Sanano T, Hirao K, Yano K, Kawabata M, Okishige K, Isobe M (2002) Delayed thrombogenesis following radiofrequency catheter ablation. Circ J 66:671–676
7. Li A, Kuga K, Suzuki A, Endo M, Niho B, Enomoto M, Kanemoto M, Yamaguchi I (2002) Effects of linear ablation at the isthmus between the tricuspid annulus and inferior vena cava for atrial flutter on autonomic nervous activity: analysis of heart rate variability. Circ J 66:53–57
8. Marrouche NF, Dresing T, Cole C, Bash D, Saad E, Balaban K, Pavia SV, Schweikert R, Saliba W, Abdul-Karim A, Pisano E, Faoelli R, Tchou P, Natale A (2002) Circular mapping and ablation of the pulmonary vein for treatment of atrial fibrillation. J Am Coll Cardiol 40:464–474
9. Tanaka K, Satake S, Saito S, Takahashi S, Hiroe Y, Mayashita Y, Tanaka S, Tanaka M, Yatanabe Y (2001) A new radiofrequency thermal balloon catheter for pulmonary vein isolation. J Am Coll Cardiol 38:2079–2086
10. Mangrum JM, Mounsey JP, Kok LC, DiMarco JP, Haines DE (2002) Intracardiac echocardiography-guided, anatomically based radiofrequency ablation of focal atrial fibrillation originating from pulmonary veins. J Am Coll Cardiol 39:1964–1972
11. Seshadri N, Novaro GM, Prieto L, White RD, Natale A, Grimm RA, Stewart WJ (2002) Pulmonary vein stenosis after catheter ablation of atrial arrhythmias. Circulation 105:2571–2572
12. Greil GF, Powell AJ, Gildein HP, Geva T (2002) Gadolinium-enhanced three-dimensional magnetic resonance angiography of pulmonary and systemic venous anomalies. J Am Coll Cardiol 39:335–341
13. Ferrari VA, Scott CH, Holland GA, Axel L, Sutton MS (2001) Ultrafast three-dimensional contrast-enhanced magnetic resonance angiography and imaging in the diagnosis of partial anomalous pulmonary venous drainage. J Am Coll Cardiol 37:1120–1128

Ras Induces Vascular Smooth Muscle Cell Senescence and Inflammation in Human Atherosclerosis

Tohru Minamino, MD, PhD*; Toshihiko Yoshida, MD, PhD*; Kaoru Tateno, MD; Hideyuki Miyauchi, MD; Yonzeng Zou, MD; Haruhiro Toko, MD; Issei Komuro, MD, PhD

Background—Vascular cells have a finite cell lifespan and eventually enter an irreversible growth arrest, cellular senescence. The functional changes associated with cellular senescence are thought to contribute to human aging and age-related vascular disorders. Ras, an important signaling molecule involved in atherogenic stimuli, is known to promote aging in yeast and cellular senescence in primary human fibroblasts. The aim of this study was to investigate the role of Ras-induced vascular smooth muscle cell (VSMC) senescence in atherogenesis.

Methods and Results—We introduced an activated *ras* allele (H-*ras*V12) into human VSMCs using retroviral infection. Introduction of H-*ras*V12 induced a growth arrest with phenotypic characteristics of cellular senescence, such as enlarged cell shapes and increases in expression of cyclin-dependent kinase inhibitors and senescence-associated β-galactosidase (SA-β-gal) activity. Activation of Ras drastically increased expression of proinflammatory cytokines, in part through extracellular signal-regulated kinase activation. To determine whether Ras activation induces cellular senescence in vivo, we transduced the adenoviral vector encoding H-*ras*V12 into rat carotid arteries injured by a balloon catheter. Introduction of Ras into the arteries enhanced vascular inflammation and senescence compared with mock-infected injured arteries. Moreover, SA-β-gal–positive VSMCs were detected in the intima of advanced human atherosclerotic lesions and exhibited increased levels of extracellular signal-regulated kinase activity and proinflammatory cytokine expression.

Conclusions—Our results suggest that atherogenic stimuli mediated by Ras induce VSMC senescence and vascular inflammation, thereby contributing to atherogenesis. This novel mechanism of atherogenesis may provide insights into a new antisenescence treatment for atherosclerosis. (***Circulation***. 2003;108:●●●-●●●.)

Key Words: aging ■ inflammation ■ atherosclerosis

Activation of Ras protein has been demonstrated to promote cell proliferation and transformation in immortal cell lines derived from various types of mammalian cells and thus has been thought to contribute to tumorigenesis in humans.[1,2] In yeast, however, loss-of-function mutations in the Ras signaling pathway have been shown to extend longevity, which indicates that Ras activity negatively controls lifespan.[3] Recently, in primary human fibroblasts, constitutive activation of the Ras signaling pathway has been reported to provoke cellular senescence, originally defined as a phenotype of arrested cells at the end of the replicative lifespan.[4-6]

Cellular senescence is accompanied by a specific set of changes in cell function, morphology, and gene expression. A number of studies have indicated that many of the changes in senescent vascular cell behavior are consistent with known changes seen in age-related vascular diseases including atherosclerosis, which suggests that these changes in cell phenotype may contribute to atherogenesis.[7] In addition, it has been reported that enlarged vascular cells that resemble senescent cells in vitro are frequently found in human atherosclerotic plaque and that in vitro growth properties of vascular cells isolated from atherosclerotic lesions are impaired compared with normal lesions, which implies that vascular cell senescence might occur in vivo.[8,9]

Consistent with this notion, we have demonstrated previously that senescent vascular endothelial cells are predominately localized in the plaque of human atherosclerosis but not in normal lesions and that vascular cell senescence results in endothelial dysfunction.[10] Given that various atherogenic stimuli, including growth factors and oxidative stress, are mediated by Ras activity,[11,12] it is assumed that activation of Ras promotes vascular cell senescence, thereby contributing to the pathogenesis of human atherosclerosis.

In the present study, we provide evidence that activation of Ras is involved in atherogenesis by inducing vascular smooth

Received April 28, 2003; revision received July 15, 2003; accepted July 16, 2003.
From the Department of Cardiovascular Science and Medicine, Chiba University Graduate School of Medicine, Chiba, Japan.
*Drs Minamino and Yoshida contributed equally to this work.
Supplemental Methods information and Figures I through VIII are available in the online-only Data Supplement at http://www.circulationaha.org.
Correspondence to Issei Komuro, MD, PhD, Department of Cardiovascular Science and Medicine, Chiba University Graduate School of Medicine, 1-8-1 Inohana, Chuo-ku, Chiba 260-8670, Japan. E-mail komuro-tky@umin.ac.jp

Circulation **is available at http://www.circulationaha.org** **DOI: 10.1161/01.CIR.0000093274.82929.22**

muscle cell (VSMC) senescence. Constitutive activation of Ras promoted cellular senescence and drastically induced expression of proinflammatory cytokines in the primary cultures of human vascular cells, in part through extracellular signal-regulated kinase (ERK) activation. Introduction of Ras into the injured arteries enhanced vascular inflammation and senescence. Furthermore, activation of ERK and vascular inflammation were associated with VSMC senescence in human atherosclerosis, which suggests that Ras activity plays an important role in regulating VSMC lifespan and function in vivo.

Methods

Tissue Specimens

Advanced human atherosclerotic samples were obtained during surgery from 6 patients who had abdominal aortic aneurysm or peripheral arterial disease with their permission and subjected to senescence-associated β-galactosidase (SA-β-gal) staining within 3 hours after excision. Gastroepiploic arteries were obtained from 3 patients with an age range of 32 to 40 years who underwent gastric resection because of gastric cancer and used as normal control samples. The studies on human samples were approved by our institutional review board.

Histology

SA-β-gal activity was examined in tissue as described previously.[13] Immunohistochemical analyses of the frozen sections (6 μm) were performed as described previously.[10] Antibodies used were as follows: antibodies to phospho-ERK and interleukin (IL)-1β (Santa Cruz), anti-α-smooth muscle actin antibody for VSMCs (Pharmingen), and anti-CD68 antibody for macrophages (DAKO).

Retroviral Infection

Primary cultures of human aortic VSMCs were purchased from BioWhittaker and cultured according to the manufacturer's instructions. Retroviral vector encoding H-*ras*V12 (pBabeH-*ras*V12) was the kind gift of Dr S.W. Lowe (Cold Spring Harbor Laboratory, Cold Spring Harbor, NY). Retroviral stocks were generated by transient transfection of packaging cell line (PT67, Clontech) with the empty vector, pBabe (mock), or pBabeH-*ras*V12 as described previously.[14]

In Vivo *H-ras*V12 Gene Transfer

A cDNA fragment encoding the H-*ras*V12 gene was cloned into a shuttle plasmid (pShuttle, Clonthech), the excised fragment derived from the shuttle plasmid was then cloned into pAdeno-X (Clontech), and high-titer adenoviral stock was generated according to the user's manual for Adeno-X Expression System. Rat carotid injury model was prepared as described previously.[15] After denudation, the H-*ras*V12 adenoviral vector or the empty adenoviral vector (5×10^9 pfu/mL) was introduced into injured arteries. Two weeks after transduction, injured arteries were perfused with saline to remove blood cells from the lumen and analyzed for vascular inflammation. The experimental protocol for the present study was designed in accordance with the "Guide for Animal Experimentation," Chiba University.

Methods for Western blot and Northern blot are available in the Online Data Supplement.

Results

Activation of Ras Promotes VSMC Senescence

We first determined whether activation of Ras induces cellular senescence in VSMCs. We introduced an activated *ras* allele (H-*ras*V12) into human VSMCs using retroviral infection and compared these with VSMCs infected with the empty vector, pBabe (mock). Transduced cells were then purified by use of puromycin for 4 days. After selection, 3×10^5 cells were seeded onto a 100-mm-diameter dish on the fifth day (designated day 0) and subjected to analyses for cell morphology, cell growth, and gene expression. H-*ras*V12–transduced VSMCs became flat and enlarged in morphology, a characteristic of the senescent phenotype, and were apparently growth arrested by day 3, whereas mock-infected VSMCs exhibited normal morphology and growth (Figures 1A and 2A). To ascertain whether Ras activation results in senescence, we examined SA-β-gal activity, a biomarker for cellular senescence. Increased activity of SA-β-gal has been reported in senescent human fibroblasts when assayed at pH 6, which is distinguishable from endogenous lysosomal β-gal activity that can be detected at pH 4. It has been shown that when applied to human dermal tissues from donors with an age range of 20 to 90 years, there is a clear correlation between the number of senescent (SA-β-gal positive) cells and the age of donor tissue.[13] SA-β-gal activity was significantly increased in H-*ras*V12–transduced VSMCs ($P<0.005$; Figure 1A and Data Supplement Figure I), which indicates that activation of Ras promoted cellular senescence in human VSMCs. To characterize the nature of cell cycle arrest caused

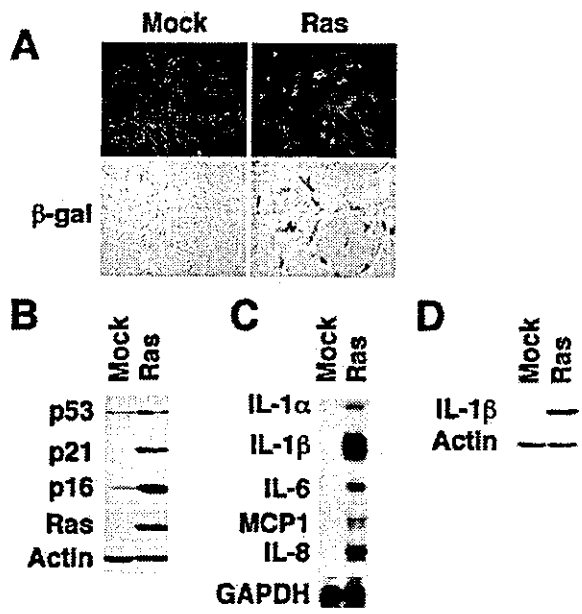

Figure 1. Activation of Ras induces premature senescence and proinflammatory molecules in human VSMCs. A, Cell morphology and SA-β-gal activity. H-*ras*V12–transduced VSMCs became flat and enlarged by day 3 (top, Ras) compared with VSMCs infected with empty vector, pBabe (top, Mock), which resulted in increased activity of SA-β-gal (bottom, β-gal). B, Expression of cell-cycle regulatory proteins. Whole-cell lysates were extracted from H-*ras*V12–transduced (Ras) or mock-transduced (Mock) VSMCs on day 0 and examined for cell-cycle regulatory proteins by Western blot analyses. C and D, Expression of proinflammatory molecules. Total RNA samples or whole-cell lysates were extracted from H-*ras*V12–transduced (Ras) or mock-transduced (Mock) VSMCs on day 3 and analyzed for proinflammatory cytokines and chemokines by ribonuclease protection assay (C) and Western blotting (D). Expression levels of GAPDH or actin served as internal controls. Similar results were obtained from 3 independent experiments.

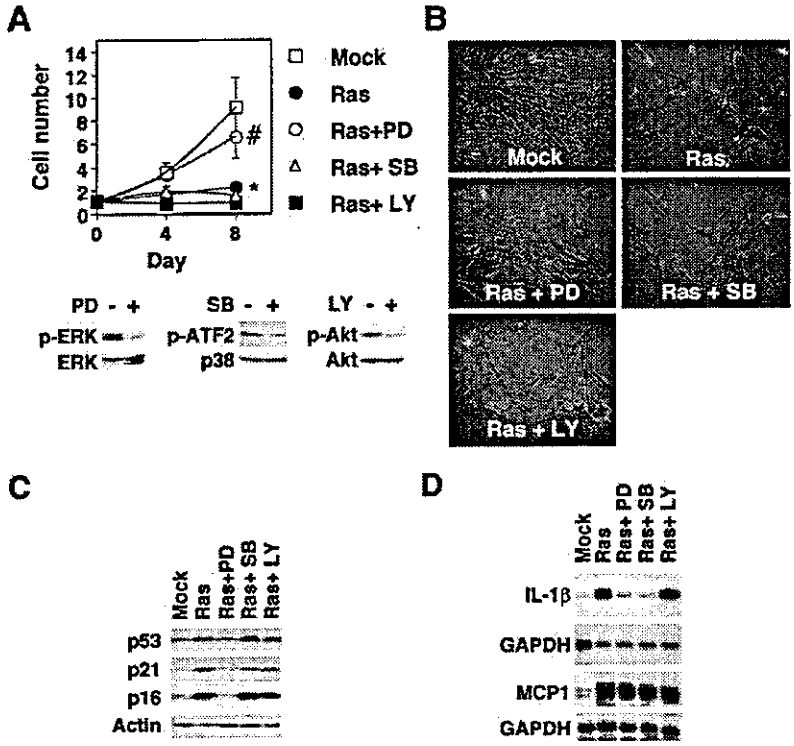

Figure 2. Role of ERK activation in Ras-induced VSMC senescence and vascular inflammation in vitro. A, Effects of kinase inhibitors on cell growth after infection with H-*ras*V12. Human VSMCs infected with pBabe or pBabeH-*ras*V12 were purified with puromycin in absence (Mock, Ras) or presence of PD98059 (Ras+PD, 50 μmol/L), LY294002 (Ras+LY, 20 μmol/L), or SB203580 (Ras+SB, 50 μmol/L), and 3×10^5 cells were plated on day 0. Treatments with kinase inhibitors were started 2 days after infection and continued until cells were harvested. Cell number was then counted at indicated time points (n=4). Cell number on day 0 (3×10^5 cells) was set at 1, and relative cell number was plotted in graph (*$P<0.001$ vs Mock, #$P<0.001$ vs Ras, n=4, ANOVA). Inhibition of each signaling cascade by kinase inhibitor was verified by Western blotting analyses. B, Cell morphology of Ras-infected VSMCs after treatment with kinase inhibitors. Original magnification was ×40. C, Expression of cell-cycle regulatory proteins after treatment with kinase inhibitors. Human VSMCs infected with pBabe or pBabeH-*ras*V12 were cultured in absence (Mock, Ras) or presence of PD98059 (Ras+PD), LY294002 (Ras+LY), or SB203580 (Ras+SB) as described above. Whole-cell lysates were extracted on day 0 and examined for cell-cycle regulatory proteins by Western blot analyses. Similar results were observed in 3 independent Western blot analyses. D, Expression of proinflammatory molecules after treatment with kinase inhibitors. Human VSMCs infected with pBabe or pBabeH-*ras*V12 were cultured in absence (Mock, Ras) or presence of PD98059 (Ras+PD), LY294002 (Ras+LY), or SB203580 (Ras+SB). Total RNA samples were extracted from cell populations on day 3 and analyzed for proinflammatory cytokines and chemokines by ribonuclease protection assay. Similar results were obtained from 3 independent experiments.

by H-*ras*V12, we examined expression of cell-cycle regulatory proteins. We found that Ras activation resulted in elevated expression of p53 (2-fold, $P<0.05$) and p21 (17-fold, $P<0.01$) as well as p16 (5-fold, $P<0.01$; Figure 1B and Data Supplement Figure II), which suggests that Ras-induced growth arrest is different from quiescence, because neither p53 nor p16 accumulates during quiescence.

Ras Activation Induces Proinflammatory Cytokines

Atherosclerosis is characterized by the recruitment of monocytes into arterial walls, and this process involves various proinflammatory molecules such as cytokines and chemokines.[16] To investigate the role of Ras-induced cellular senescence in atherogenesis, we examined expression of proinflammatory cytokines and chemokines in human VSMCs. Introduction of H-*ras*V12 drastically induced expression levels of proinflammatory cytokines and chemokines such as IL-1α (11-fold, $P<0.05$), IL-1β (50-fold, $P<0.01$), IL-6 (12-fold, $P<0.05$), IL-8 (77-fold, $P<0.01$), and monocyte chemoattractant protein (MCP)-1 (6-fold, $P<0.05$) as demonstrated by ribonuclease protection assay and Western blot analysis compared with mock-infected VSMCs (Figures 1C and 1D and Data Supplement Figure III). These results suggest that activation of Ras may induce vascular inflammation in human atherosclerosis. Expression of proinflammatory cytokines was also elevated in VSMCs undergoing replicative senescence compared with young cell populations, although the increased levels were <10-fold (Data Supplement Figure IV).

Role of ERK Activation in Ras-Induced VSMC Senescence and Inflammation

We next investigated the potential downstream signaling pathways that are activated by H-*ras*V12 to promote VSMC senescence. A number of signaling cascades have been implicated in cell survival and cell growth induced by Ras

activation, including mitogen-activated protein kinase kinase (MEK)/extracellular signal-regulated kinase (ERK), phosphatidylinositol 3-kinase (PI3K)/Akt, and p38.[1,2] H-*ras*V12–transduced VSMCs were analyzed for cell growth in the presence of specific kinase inhibitors: PD98059 for MEK1/ERK, LY294002 for PI3K/Akt, or SB203580 for p38. Inhibition of each signaling cascade by the kinase inhibitor was verified by Western blot analyses for phospho-ERK (PD98059), phospho-Akt (LY294002), and phospho-ATF-2, which is known to be phosphorylated by p38 (SB203580; Figure 2A). Introduction of H-*ras*V12 resulted in growth arrest compared with mock-infected cells ($P<0.001$), and treatment with PD98059 but neither LY294002 or SB203580 significantly ameliorated the growth-inhibitory effects of Ras activation in VSMCs ($P<0.001$ versus Ras; Figure 2A). In addition, inhibition of the MEK/ERK signaling pathway prevented morphological changes induced by Ras activation, whereas inhibition of either the PI3K/Akt or p38 pathway had no effect (Figure 2B), which suggests that the MEK/ERK signaling pathway is involved in Ras-induced VSMC senescence. This idea is further supported by Western blot analyses for cell-cycle regulatory proteins. Increased expression of p53, p21, and p16 by H-*ras*V12 transduction was effectively inhibited by PD98059 ($P<0.05$ for p53 and p21, $P<0.01$ for p16 versus Ras) but not by either LY294002 or SB203580 (Figure 2C and Data Supplement Figure V). To elucidate the signaling pathways that contribute to Ras-induced cytokine expression, we performed ribonuclease protection assay in H-*ras*V12–infected VSMCs treated with the kinase inhibitors. Treatment with either PD98059 or SB203580 but not LY294002 significantly reduced expression levels of IL-1β ($P<0.01$ versus Ras) in Ras-infected VSMCs (Figure 2D, upper panel, and Data Supplement Figure VI). In contrast, all kinase inhibitors examined had no effect on expression of MCP-1 (Figure 2D, lower panel, and Data Supplement Figure VI). Thus, these data suggest that the MEK/ERK signaling pathway is important for Ras-induced cell growth arrest, but there are other pathways for vascular inflammatory response elicited by Ras activation.

Activation of Ras Induces VSMC Senescence and Inflammation In Vivo

To determine whether Ras activation induces cellular senescence and inflammation in vivo, we transduced the adenoviral vector encoding H-*ras*V12 (AdenoRas) or the empty vector (mock) into rat carotid arteries injured by a balloon catheter. We chose a rat carotid injury model for analysis of vascular inflammation because it is known that accumulation of macrophages is minimally involved in lesion formation in this model. Two weeks after transduction, injured arteries were analyzed for SA-β-gal activity. Whereas only a little SA-β-gal activity was found in mock-infected injured arteries, transduction of AdenoRas into injured arteries increased SA-β-gal activity (Figure 3A, left). Immunohistochemical analyses indicated that these SA-β-gal–positive cells were VSMCs in the outer layer of the intima and the media (Figure 3A, right), which suggests that activation of Ras induced VSMC senescence in vivo as well. We also observed a weak SA-β-gal staining in the inner layer of the intimal VSMCs

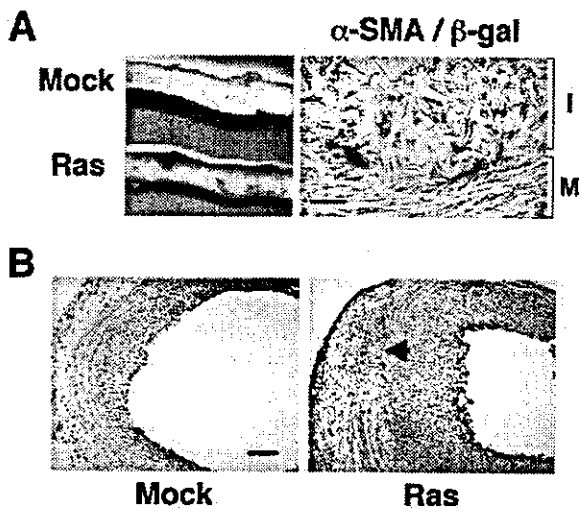

Figure 3. Activation of Ras induces VSMC senescence and vascular inflammation in vivo. A, SA-β-gal activity in injured arteries. Left panel shows photograph of injured arteries stained with β-gal staining. Whereas only a little SA-β-gal activity was found in injured arteries infected with empty vector (Mock), transduction of AdenoRas into injured arteries increased SA-β-gal activity (Ras). Double staining for α-smooth muscle actin (brown) and SA-β-gal activity (blue) of AdenoRas-infected injured arteries indicates that these β-gal-positive cells were VSMCs in outer layer of intima (I) and media (M; right). Original magnification was ×1000. Scale bar=10 μm. B, Immunohistochemistry for macrophages in injured arteries. Two weeks after vascular injury and infection with empty vector or AdenoRas, arteries were perfused with saline to remove blood cells from lumen and analyzed for vascular inflammation. Accumulation of macrophages (brown) was markedly enhanced in AdenoRas-infected injured arteries (Ras) compared with injured arteries infected with empty vector (Mock). Arrowhead indicates disruption of media in AdenoRas-infected arteries. Original magnification was ×100. Scale bar=100 μm.

(data not shown). Furthermore, the area of accumulated macrophages in the intima was increased markedly (~8-fold, $P<0.001$) in AdenoRas-infected injured arteries compared with mock-infected injured arteries (Figure 3B and Data Supplement Figure VII), which indicates a causal relationship between Ras activation and vascular inflammation. Disruption of medial layers, one of the pathological features of human atheroma, was observed frequently in AdenoRas-infected injured arteries, whereas it was never detected in mock-infected injured arteries, further implicating a critical role of Ras activation in atherogenesis.

Senescent VSMCs in Advanced Human Atherosclerotic Plaque

To investigate the possible role of Ras-induced VSMC senescence in human atherosclerosis, we first examined SA-β-gal activity to locate senescent VSMCs in advanced human atherosclerotic plaque. Many of the intimal cells exhibited granular blue stainings in the cytoplasm that were quite similar to those of senescent cells in culture reported previously (Figure 4A).[13] Double staining for α-smooth muscle actin and SA-β-gal activity identified SA-β-gal–positive cells as VSMCs in the intima (Figure 4A). No signal

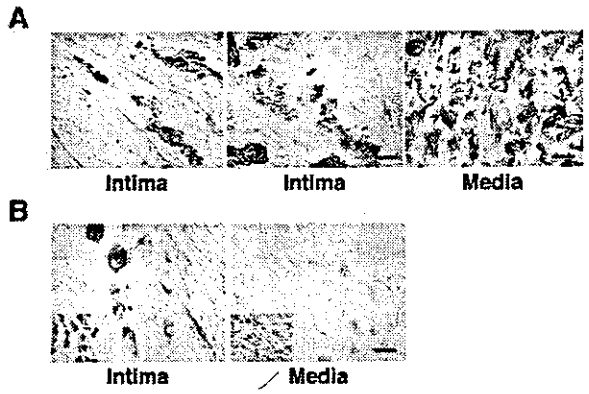

Figure 4. Senescent VSMCs in advanced human atherosclerosis. A, Double staining for α-smooth muscle actin (brown) and SA-β-gal activity (blue) in intima and media. Many intimal cells exhibited granular blue stainings in cytoplasm that are colocalized with immunoreactivity of α-smooth muscle actin (Intima). In contrast, few SA-β-gal–positive VSMCs were observed in media (Media). Nuclei were counterstained with hematoxylin and are shown in purple. Original magnification was ×1000. Scale bars=10 μm. All samples examined provided similar results. B, Activation of ERK in senescent VSMCs in human atherosclerosis. Cross sections of atherosclerotic samples were double stained with β-gal activity and anti-phospho-ERK. Activated ERK (brown) was detected in nucleus of β-gal–positive VSMCs in intima (Intima), whereas few medial VSMCs exhibited ERK activation (Media). Original magnification was ×1000. Scale bars=10 μm. Insets show immunostaining for α-smooth muscle actin of serial sections.

was detected in a control staining with nonimmune IgG (data not shown). To ascertain whether SA-β-gal–positive cells in the intima were senescent VSMCs, we performed a double staining for p53 and SA-β-gal activity. Whereas neither SA-β-gal activity nor p53 expression was observed in medial VSMCs, SA-β-gal–positive cells in the intima revealed p53 immunoreactivity in the nucleus (Figure 4A and Data Supplement Figure VIII), which suggests that these cells were likely VSMCs with senescence-associated phenotypes.

We next determined whether activation of the Ras/MEK/ERK signaling pathway accounts for VSMC senescence in human atherosclerosis. We performed an immunostaining with anti-phospho-ERK antibody in advanced human atherosclerotic plaque. Activated ERK was found in the nucleus and to a lesser extent in the cytoplasm of intimal VSMCs, whereas few medial VSMCs exhibited ERK activation (Figure 4B). No signal was observed in control staining with nonimmune IgG (data not shown). More importantly, activated ERK was often colocalized with SA-β-gal activity in intimal VSMCs (Figure 4B), which implies a critical role of the Ras/MEK/ERK signaling pathway in VSMC senescence in human atherosclerotic plaque. SA-β-gal–positive VSMCs were frequently found in the regions adjacent to infiltrated macrophages, which indicates a possible role of VSMC senescence in vascular inflammation.

Senescent VSMCs Express Proinflammatory Molecules in Human Atherosclerosis

To ascertain whether VSMC senescence induces vascular inflammation in human atherosclerosis, we performed an immunostaining for IL-1β in human advanced atherosclerosis. IL-1β expression was detected in the intima of advanced lesions but not in normal lesions (Figure 5 and data not shown). No signal was detected in a control staining with nonimmune IgG (data not shown). Furthermore, expression of IL-1β was colocalized with SA-β-gal activity in intimal VSMCs, whereas VSMCs negative for SA-β-gal activity in the media did not express IL-1β (Figure 5), which suggests that VSMC senescence may induce expression of proinflammatory cytokines in human atherosclerotic lesions.

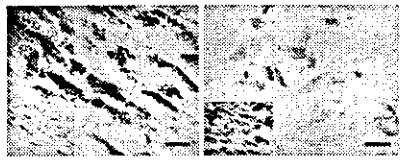

Figure 5. Senescent VSMCs express proinflammatory cytokines in human atherosclerosis. Cross sections of atherosclerotic samples were immunostained with anti-IL-1β antibody. Expression of IL-1β (brown) was colocalized with SA-β-gal activity (blue) in intimal VSMCs (Intima), whereas SA-β-gal–negative VSMCs in media did not express IL-1β (Media). Insets show immunostaining for α-smooth muscle actin of serial sections. Original magnification was ×1000. Scale bars=10 μm.

Discussion

It has been demonstrated that various molecules including growth factors, vasoactive peptides, and oxidative stress are induced during lesion formation and regulate numerous critical cell functions, thereby contributing to atherogenesis.[17] These stimuli function as mitogens for VSMCs through the signaling cascades that activate Ras. Inhibition of Ras activity has been reported to prevent intimal formation after vascular injury, which suggests a critical role of Ras activation in VSMC proliferation.[18] In the present study, the cell number of Ras-infected VSMCs was ~1.5-fold more than that of mock-infected VSMCs on the third day after infection (T. Minamino, unpublished observation, 2002). However, Ras-infected cells were virtually growth arrested by day 3 (the eighth day after infection), whereas mock-infected cells were being proliferated (Figure 2A). Thus, it is likely that introduction of Ras initially promotes VSMC proliferation, and when constitutively activated, Ras induces VSMC senescence. This notion was further supported by the fact that senescent VSMCs were detected in advanced human atheroma but not in early lesions of atherosclerosis.[10]

The present data provide evidence that constitutive activation of Ras induces vascular inflammation and senescence in vitro and in vivo. Consistent with our findings, functional inhibition of Ras has been demonstrated to suppress expression of proinflammatory molecules, thereby reducing lesion formation in apolipoprotein E-deficient mice.[19] Moreover, angiotensin II, an important atherogenic molecule that activates the Ras signaling pathway, has been demonstrated to promote VSMC senescence and vascular inflammation.[20] We found that treatment of human VSMCs with proinflammatory cytokines did not induce premature senescence (T. Minamino, unpublished observation). Thus, it is likely that increased

expression of proinflammatory molecules is a result of cellular senescence rather than a cause. Vascular inflammation is known to promote degradation of extracellular matrix by various proteinases such as collagenases and gelatinases and by inhibition of matrix production.[21] Therefore, it is assumed that decreased cellularity and enhanced inflammation associated with VSMC senescence may contribute to plaque vulnerability.

The growth signals mediated by Ras are known to promote aging in yeast.[3] The present results suggest that the signaling pathway of cellular aging is conserved in human VSMCs and that constitutive mitogenic stimuli in the lesions induce a senescent phenotype in VSMCs, thereby contributing to atherogenesis. Gain-of-function mutation of Ras has been found frequently in human malignancy, whereas introduction of oncogenic Ras into human primary cultures results in cellular senescence. Thus, Ras-induced senescence is thought to be an antitumorigenic mechanism in normal somatic cells.[22] Ras-induced growth arrest may have beneficial effects early in life to decrease the incidence of cancer, but late in life, this mechanism may promote the accumulation of senescent cells in a body, which results in age-associated diseases such as atherosclerosis.

In summary, we demonstrated the role of Ras-induced VSMC senescence in vitro and in vivo. Introduction of senescence by activation of Ras resulted in vascular inflammation, whereas inhibition of senescence reduced the inflammatory response. Activation of ERK and increased expression of proinflammatory cytokines were detected in senescent VSMCs in human atherosclerosis. We propose a novel mechanism of atherogenesis whereby atherogenic stimuli promote VSMC senescence by activating Ras, which in turn results in induction of proinflammatory cytokines and chemokines, leading to further vascular inflammation. Thus, our results will provide insights into a novel antisenescence treatment for atherosclerosis.

Acknowledgments

This work was supported by grants from Takeda Medical Research Foundation, Takeda Science Foundation, Japan Heart Foundation, Mochida Memorial Foundation, Uehara Memorial Foundation, Mitsubishi Pharma Research Foundation, and the Ministry of Education, Science, Sports, and Culture of Japan (to Drs Minamino and Komuro). We thank Dr Lowe for pBabeH*ras*V12.

References

1. Bar-Sagi D, Hall A. Ras and Rho GTPases: a family reunion. *Cell.* 2000;103:227–238.
2. Frame S, Balmain A. Integration of positive and negative growth signals during ras pathway activation in vivo. *Curr Opin Genet Dev.* 2000;10:106–113.
3. Kenyon C. A conserved regulatory system for aging. *Cell.* 2001;105:165–168.
4. Serrano M, Lin AW, McCurrach ME, et al. Oncogenic ras provokes premature cell senescence associated with accumulation of p53 and p16INK4a. *Cell.* 1997;88:593–602.
5. Lin AW, Barradas M, Stone JC, et al. Premature senescence involving p53 and p16 is activated in response to constitutive MEK/MAPK mitogenic signaling. *Genes Dev.* 1998;12:3008–3019.
6. Zhu J, Woods D, McMahon M, et al. Senescence of human fibroblasts induced by oncogenic Raf. *Genes Dev.* 1998;12:2997–3007.
7. Cooper LT, Cooke JP, Dzau VJ. The vasculopathy of aging. *J Gerontol.* 1994;49:B191–B196.
8. Ross R, Wight TN, Strandness E, et al. Human atherosclerosis, I: cell constitution and characteristics of advanced lesions of the superficial femoral artery. *Am J Pathol.* 1984;114:79–93.
9. Bennett MR, Macdonald K, Chan SW, et al. Cooperative interactions between RB and p53 regulate cell proliferation, cell senescence, and apoptosis in human vascular smooth muscle cells from atherosclerotic plaques. *Circ Res.* 1998;82:704–712.
10. Minamino T, Miyauchi H, Yoshida T, et al. Endothelial cell senescence in human atherosclerosis: role of telomere in endothelial dysfunction. *Circulation.* 2002;105:1541–1544.
11. Benjamin CW, Jones DA. Platelet-derived growth factor stimulates growth factor receptor binding protein-2 association with Shc in vascular smooth muscle cells. *J Biol Chem.* 1994;269:30911–30916.
12. Deguchi J, Makuuchi M, Nakaoka T, et al. Angiotensin II stimulates platelet-derived growth factor-B chain expression in newborn rat vascular smooth muscle cells and neointimal cells through Ras, extracellular signal-regulated protein kinase, and c-Jun N-terminal protein kinase mechanisms. *Circ Res.* 1999;85:565–574.
13. Dimri GP, Lee X, Basile G, et al. A biomarker that identifies senescent human cells in culture and in aging skin in vivo. *Proc Natl Acad Sci USA.* 1995;92:9363–9367.
14. Minamino T, Mitsialis SA, Kourembanas S. Hypoxia extends the life span of vascular smooth muscle cells through telomerase activation. *Mol Cell Biol.* 2001;21:3336–3342.
15. Minamino T, Kurihara H, Takahashi M, et al. Endothelin-converting enzyme expression in the rat vascular injury model and human coronary atherosclerosis. *Circulation.* 1997;95:221–230.
16. Lusis AJ. Atherosclerosis. *Nature.* 2000;407:233–241.
17. Ross R. Cell biology of atherosclerosis. *Annu Rev Physiol.* 1995;57:791–804.
18. Indolfi C, Avvedimento EV, Rapacciuolo A, et al. Inhibition of cellular ras prevents smooth muscle cell proliferation after vascular injury in vivo. *Nat Med.* 1995;1:541–545.
19. George J, Afek A, Keren P, et al. Functional inhibition of Ras by S-trans, trans-farnesyl thiosalicylic acid attenuates atherosclerosis in apolipoprotein E knockout mice. *Circulation.* 2002;105:2416–2422.
20. Brasier AR, Recinos A III, Eledrisi MS. Vascular inflammation and the renin-angiotensin system. *Arterioscler Thromb Vasc Biol.* 2002;22:1257–1266.
21. Libby P, Ridker PM, Maseri A. Inflammation and atherosclerosis. *Circulation.* 2002;105:1135–1143.
22. Campisi J. Cellular senescence as a tumor-suppressor mechanism. *Trends Cell Biol.* 2001;11:S27–S31.

Nucleic Acids Research, 2003, Vol. 31, No. 20 ***5941–5948***
DOI: 10.1093/nar/gkg807

Sox6 regulation of cardiac myocyte development

Orit Cohen-Barak, Zanhua Yi, Nobuko Hagiwara[1], Koshiro Monzen[2], Issei Komuro[3] and Murray H. Brilliant*

Department of Pediatrics, The University of Arizona College of Medicine, Steele Memorial Children's Research Center 1501 N. Campbell Avenue, Tucson, AZ 85724, USA, [1]Division of Cardiovascular Medicine, Rowe Program in Genetics, University of California, Davis, CA 95616, USA, [2]Department of Cardiovascular Medicine and Department of Clinical Bioinformatics, University of Tokyo Graduate School of Medicine, Tokyo 113-8655, Japan and [3]Department of Cardiovascular Science and Medicine, Chiba University Graduate School of Medicine, Chiba 260-8670, Japan

Received July 7, 2003; Revised August 22, 2003; Accepted September 2, 2003

ABSTRACT

A mouse mutation (p^{100H}/p^{100H}) has been identified that is associated with cardioskeletal myopathy, heart block, delayed growth and early postnatal death. The gene that is disrupted in this mutation encodes the transcription factor *Sox6*. P19CL6 cells were used as an *in vitro* cardiomyocyte differentiation system and revealed that *Sox6* is expressed exclusively when the cells are committed to differentiate to beating cardiac myocytes. We used the yeast two-hybrid system to identify the Prtb (*Proline-rich transcript of the brain*) protein as a Sox6 interactor, and subsequently confirmed the interaction by co-immunoprecipitation. *Prtb* expression in P19CL6 cells increased with differentiation to beating cardiomyocytes. Using the P19CL6 cells stably transfected with noggin, an antagonist of BMP (Bone Morphogenic Protein), we found that BMP expression is required for Sox6 expression in cardiomyocyte differentiation. Surprisingly, the expression of the α_{1c}-subunit gene of the L-type Ca^{2+} channel decreased in P19CL6 cells as they differentiated to beating cardiac cells. Ectopic expression of *Sox6* or *Prtb* alone in P19CL6 cells caused down-regulation of L-type Ca^{2+} α_{1c} expression, but when *Sox6* and *Prtb* were co-transfected to the cells, L-type Ca^{2+} α_{1c} remained at basal levels. A similar relationship of Sox6 and L-type Ca^{2+} α_{1c} expression was seen *in vivo* (comparing wild-type and p^{100H}/p^{100H} mutant mice). Thus, Sox6 is within the BMP pathway in cardiac differentiation, interacts with Prtb and may play a critical role in the regulation of a cardiac L-type Ca^{2+} channel.

INTRODUCTION

In distinct muscle cell lineages, individual muscle-specific genes exhibit unique temporal-spatial patterns of expression. Regulatory programs for myocyte transcription result from developmental cues and positional information that are mediated by specific transcription factors. The transcriptional expression pattern of muscle-specific genes is ultimately dependent on combinatorial interactions among the transcription factors that bind different regulatory proteins (1).

The *Sox* (*Sry* related HMG box) gene family encodes an important group of transcription factors that are key regulators of embryonic development and cell fate determination (2). Mutations of *Sox6*, a member of this family, are associated with neonatal lethality in the mouse (3,4). *Sox6* was initially isolated from an adult mouse testis cDNA library (5), but its functional significance in this tissue is unknown. Sox6 has been suggested to play a role in the development of the central nervous system (5), chondrogenesis (4,6–8) and cardiac and skeletal muscle cell maintenance (3). Mice homozygous for a *Sox6* null mutation, p^{100H}, show delayed growth and die within 2 weeks after birth (3). Analysis of the p^{100H} phenotype revealed that the p^{100H} mutant develops myopathy and arterioventricular (AV) heart block, a cardiac conduction defect associated with lethality in human cardiac myopathies (9). Thus, among its diverse functions, the Sox6 protein is likely to be involved in maintaining the normal physiological function of muscle tissue, including the heart (3). We have recently cloned and sequenced the human SOX6 cDNA, isolated from a myoblast cDNA library (10). The human SOX6 protein shows 94.3% amino acid identity to mouse Sox6 throughout the gene, and 100% identity in the critical HMG box and coiled-coil domains. Northern blot analysis revealed that human SOX6, like mouse *Sox6*, is expressed in a wide variety of tissues, and is most abundantly expressed in skeletal muscle (3,10).

The muscle cell-specific effects of the Sox6 protein may be achieved by its interactions with other transcription factors. To identify Sox6 interactors in muscle cells and elucidate how the Sox6 protein achieves such remarkable cell type specificity, a yeast two-hybrid screening was performed. This identified the Prtb (Proline-rich transcript of the brain) protein as an interactor of the Sox6 protein.

To understand the role of *Sox6* in cardiac muscle development, we utilized P19CL6, a cell line that differentiates exclusively to beating cardiomyocytes in the presence of

*To whom correspondence should be addressed. Tel: +1 520 626 3305; Fax: +1 520 626 7407; Email: mhb@peds.arizona.edu

DMSO (11). *Sox6* is not expressed in untreated P19CL6 cells, but is up-regulated following DMSO exposure, reaching maximum levels when the cells have fully differentiated into beating cardiomyocytes. In addition, we found that *Sox6* is downstream of the BMP (Bone Morphogenetic Protein) pathway in the cardiac system, using P19CL6noggin, a P19CL6 cell line stably transfected with noggin that antagonizes the BMP pathway (12).

To assess the effect of Sox6 in cardiac differentiation, we characterized the expression of the L-type Ca^{2+} channel α_{1c} gene, encoding a subunit normally expressed in the heart (13). We found that the mRNA levels of the L-type Ca^{2+} channel α_{1c} gene decreased when the P19L6 cells terminally differentiate or when they are transfected with Sox6. Moreover, in *Sox6* null mutant mice (p^{100H}/p^{100H}) (3), the expression level of this calcium channel gene is ~1.5-fold higher, correlating with the *in vitro* analysis. The Sox6 interactor, Prtb, also down-regulated the expression levels of the L-type Ca^{2+} channel α_{1c} gene, whereas *Prtb* co-expressed with *Sox6* did not.

MATERIALS AND METHODS

Plasmid construction

DNA fragments for plasmid constructs were generated by PCR or RT–PCR and confirmed by sequence analysis. To construct the plasmid pGBKT7 (Clontech) as bait for the yeast two-hybrid screen and for the co-immunoprecipitation (Co-IP), an amplified PCR fragment encoding amino acids 139–304 (including the coiled-coil domain) of mouse Sox6 (GenBank accession no. U32614) was cloned in-frame into EcoRI–SalI sites. To generate the plasmid pGADT7 (Clontech) for the Co-IP, the amplified PCR fragment encoding the first 108 amino acids of the Prtb gene (GenBank accession no. AF085348), and RT–PCR of the entire gene (168 amino acids), were cloned in-frame into EcoRI–XhoI sites. For transient transfection, complete cDNAs of the mouse *Sox6* and *Prtb* genes were cloned into EcoRI, and EcoRI–XhoI, respectively, to pCDNA3.1/Zeo vector (Invitrogen) driven by the CMV promoter.

Yeast two-hybrid screening

The MATCHMAKER two-hybrid system 3 (Clontech) was used according to the supplier's protocol with the Sox6 bait plasmid, detailed above. The screened library was mouse 11 day embryo MATCHMAKER cDNA (Clontech) that was pre-transformed to the Y187 yeast strain. The two-hybrid screening of the pre-transformed library was accomplished by yeast mating using the AH109 strain containing the bait plasmid. The screening was preformed for growth on minimal medium lacking histidine (His^-) and in the presence of 2.5 mM 3-amino-1,2,4-triazole. Of 2.3×10^6 cDNAs, approximately 300 positive colonies grew on His^-. To exclude false positive clones, the 300 colonies were replicated to high stringency plates, with simultaneous selection for three reporter genes (lacking histidine and adenine and containing X-α-Gal as substrate that employs blue/white screening directly on the plate). Approximately 200 of these clones grew under high stringency. These were sequenced and evaluated by BLAST search for being in frame with the activation domain, for the potential as a transcription factor and for expression in the developing heart. Of these, one, partially encoding Prtb, was selected for further analysis.

In vitro protein–protein interaction assay

To confirm true protein interactions, we used the MATCHMAKER Co-IP kit (Clontech) for *in vitro* Co-IP, according to the supplier's protocol. The Co-IP contains two vectors: pGBKT7 (includes the mouse Sox6 coiled-coil domain), and pGADT7 (includes a library protein isolated from the yeast two-hybrid screening). These vectors contain a T7 RNA polymerase promoter and either a c-Myc or HA epitope tag, so they can be used directly in an *in vitro* transcription/translation reaction.

RNA isolation and northern blot analysis

At varying times and treatments, cells were harvested for total RNA isolation using the UltraSpec RNA Isolation kit (Biotecx). For northern blot hybridization, equal amounts of total RNA (10 μg/lane) were subjected to electrophoresis on a 1.2% agarose gel in the presence of 5.5% formaldehyde and transferred by the alkaline method to a nylon membrane (Hybond N+; Amersham). The membranes were hybridized with distinct cDNA probes obtained by PCR or RT–PCR and confirmed by sequencing. The *Sox6* probe is a mouse cDNA fragment of 575 bp including nucleotides 1353–1927 (GenBank accession no. U32614). The *Prtb* probe is a mouse cDNA fragment of 562 bp including nucleotides 15–576 (GenBank accession no. AF085348). The *Sox9* probe is a mouse cDNA fragment of 278 bp including nucleotides 1049–1326 (GenBank accession no. BC034264). The L-type $Ca^{2+}\alpha_{1c}$ probes are mouse cDNA fragments of 548 and 540 bp including nucleotides 6294–6841 and 3072–3611, respectively (GenBank accession no. NM_009781). Probes were labeled with [^{32}P]dCTP, by random primer labeling (RediprimeII; Amersham Pharmacia Biotech). The hybridization was performed in phosphate buffered 7% SDS hybridization solution (14). Blots were washed with 0.2× SSC, 1% SDS at 60°C prior to exposure to X-ray film (Kodak) at –80°C from 3 h to 6 days. Human and mouse multiple tissue northern filters were purchased from Clontech. The filters were hybridized with mouse *Prtb* cDNA nucleotides 15–576 (GenBank accession no. AF085348) following the manufacturer's protocols and exposed to X-ray film (Kodak) at –80°C for 19 h.

Cell culture and differentiation

P19CL6 and P19CL6noggin cell lines were cultured as described previously (11). To stimulate differentiation under adherent conditions, the P19CL6 and P19CL6noggin cells were plated at a density of 3.7×10^5 cells in a 60 mm tissue culture dish with medium including 1% DMSO. The medium was changed every 2 days. The P19CL6 cells started to beat after 11 days, and virtually all of the cells on the plate were beating after 14 days. Days of differentiation were numbered consecutively (i.e. day 0, no DMSO treatment; day 1, 24 h after DMSO added).

Transient transfection assay

Transient transfections were performed in a 6-well dish using FuGENE6 reagent (Roche), according to the manufacturer's protocol. Bluescript II SK(-) plasmid was used as a control. To

evaluate transfection efficiency, cells were co-transfected with a reporter vector containing the β-gal gene driven by the CMV promoter (pCMV SPORT–βgal; Invitrogen). In each well of a 6-well plate, 3.5×10^5 cells were transfected with 1 μg of pCDNA3.1/Zeo harboring *Sox6* or *Prtb* or both plasmids, and 0.5 μg of pCMV SPORT–βgal. Cells were harvested after 24 h post-transfection for RNA for northern blot analysis (as described above). The band intensities were determined with Quantity One software (GS-700 densitometer; Bio-Rad, Hercules, CA). Also at this point protein extracts were used for the β-gal assay using the β galactosidase enzyme assay kit (Promega). The experiment was repeated three times, and the statistical analysis was done using *t*-test.

RT–PCR analysis of L-type Ca^{2+} α_{1c} gene

Total RNA from embryonic day 18.5 heart was isolated from littermate wild-type and p^{100H}/p^{100H} mutant mice. One microgram of RNA, Oligo $(dT)_{12-18}$ primer and reverse transcriptase were used for cDNA production. L-type Ca^{+2} α_{1c} cDNA analysis was performed by PCR amplification of a fragment of 548 bp using the primers: MHB1401, 5′-TATCAGAGTGACAGCAGGGGCAAC-3′; and MHB1402, 5′-AGAGAGGCAGAGCGAAGGAAAC-3′. PCRs were carried out with several dilutions of cDNAs and/or over a range of amplifying cycles to insure a linear range of amplification. A fragment of the mouse GPDH gene was amplified as internal control. Amplified products were electrophoresed on a 2% agarose gel, visualized under UV light and analyzed using a densitometer (Gel Doc 1000; Bio-Rad).

RESULTS

Screening for a candidate protein that interacts with Sox6

To identify factors that interact with Sox6, we employed the yeast two-hybrid system. As bait, we used the coiled-coil domain including amino acids 139–304 of the mouse Sox6 protein. The leucine zipper motif and the Q-box create a coiled-coil domain (6) that is 100% conserved between the mouse and human SOX6, and has a 91% identity to L-Sox5 (10). This domain mediates homodimerization and heterodimerization. We screened a cDNA library from an 11-day mouse embryo, at a stage when the *Sox6* gene is already expressed (3). One cDNA clone was selected for detailed analysis based on numerous criteria (see Materials and Methods). A BLAST search revealed that this clone contained two-thirds of the *Prtb* gene, including 108 amino acids (of 168 total) at the N-terminal (15). The full size cDNA of *Prtb* was subsequently isolated by RT–PCR. Although the two-hybrid system in yeast provides an *in vivo* analysis, it does not necessarily demonstrate direct interaction between these two proteins. To verify protein–protein interaction, we applied the Co-IP technique (Fig. 1). A c-Myc epitope tag was attached to the Sox6 bait, and an HA epitope tag was attached to both the isolated Prtb fragment (108 amino acids) and the full-length protein. The tagged proteins were expressed *in vitro* and non-denatured proteins and complexes were precipitated by anti-Myc or anti-HA. The proteins and complexes were then denatured and resolved by PAGE, verifying the interaction between the Sox6 and Prtb proteins. Both the 108 amino acid

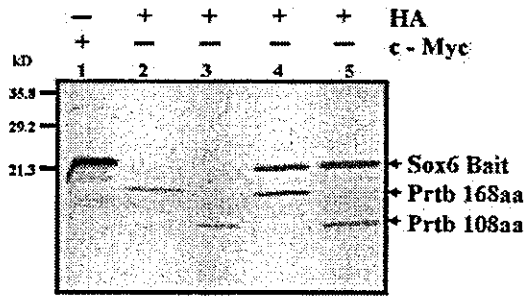

Figure 1. Protein–protein interaction assay. To verify interactions, we applied the Co-IP technique. The Sox6 bait was tagged with the a c-Myc epitope and each of the two Prtb proteins were tagged with an HA epitope. The first three lanes assay each protein by itself precipitated with an antibody to the corresponding tag. Lanes 4 and 5 assay a mix of two proteins, the Sox6 bait and one of two Prtb proteins (168 or 108 aa, lanes 4 and 5, respectively) allowed to associate prior to precipitation with the HA antibody. The antibody pulled down HA-tagged Prtb proteins and Sox6. Standard marker fragments in kDa are indicated at the left.

Prtb peptide and the full-length protein were co-precipitated with Sox6, confirming the yeast two-hybrid system results (data not shown).

The Prtb protein has no known function. An analysis using the PROSITE motif search showed a possible 'paired box' domain (16) that may function in sequence-specific DNA recognition (17). There is a 92% sequence identity between the human and mouse *Prtb* genes. This high conservation between the two species may suggest a shared, and perhaps crucial, function of this protein. *Prtb* is expressed in various levels in a variety of tissues. The expression patterns of *Prtb* in human and in mouse are shown in Figure 2A and B, respectively. In both organisms *Prtb* is expressed at high levels in the heart, and at lower levels in skeletal muscle (when compared with Sox6) (3,10).

Sox6 and *Prtb* expression during differentiation of P19CL6 cells and P19CL6noggin cells

Cardiomyocyte differentiation can be studied *in vitro* using P19CL6 cells (11), a clonal derivative of P19 murine embryonal carcinoma cells (18). Unlike the parental P19 cells, this subline efficiently differentiates into beating cardiomyocytes under adherent conditions when treated with DMSO. This cell line expresses BMPs that have been shown to play a pivotal role in the induction of the cardiac cell lineage (19,20). To further investigate the functions of BMP in cardiac development, Monzen *et al.* (12) established a variant P19CL6 cell line, P19CL6noggin, that constitutively over-expresses noggin, an antagonist of BMP. Because of the continual presence of noggin in P19CL6noggin cells, myogenic induction is suppressed and neither cardiac transcription factors nor contractile protein genes are expressed. To understand where in the cardiomyocyte developmental pathway Sox6 and Prtb may be acting, we used P19CL6 and P19CL6noggin to analyze the expression of these genes. The mRNA of *Sox6* is only detected when the cells are beating (Fig. 3) or committed to differentiate (Fig. 4). *Sox6* mRNA was not detected in untreated or DMSO treated P19CL6noggin cells that do not differentiate into cardiomyocytes (Fig. 3). These results indicate that the expression of Sox6 in P19CL6 is associated

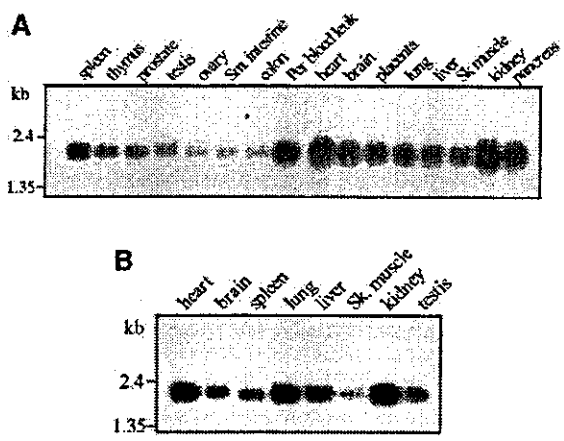

Figure 2. Human (A) and mouse (B) multiple tissue northern blots. Each lane contains 2 μg of poly(A)$^+$ RNA from the tissues indicated above. The filters were hybridized with a ^{32}P-labeled 562 bp mouse *Prtb* cDNA fragment (nucleotides 15–576). Control hybridization with β-actin was performed to confirm equal loading of RNAs (data not shown). Abbreviations used: sm. intestine, small intestine; per. blood leuk., peripheral blood leukocyte; sk. muscle, skeletal muscle; colon (mucosal lining). Standard marker fragments in kb are indicated at the left.

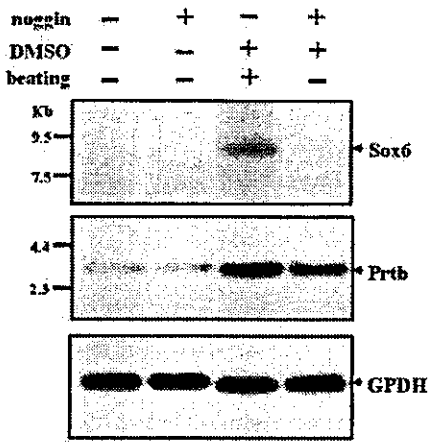

Figure 3. The expression of *Sox6* and *Prtb* in P19CL6 and P19CL6noggin cells, with or without DMSO induction. Each lane contains 10 μg of total RNA from the cells treated as labeled (above). The same filter was serially hybridized with the probes indicated on the right. Hybridization with GPDH is presented to show that the same amount of intact RNA was loaded in each lane. Standard marker fragments in kb are indicated at the left.

with the initiation of the cardiomyogenic program and not with the DMSO treatment itself. In contrast to the *Sox6* expression in P19CL6, the expression of *Prtb* is less affected by the presence of noggin, since *Prtb* is expressed in both P19CL6 and P19CL6noggin cells (Fig. 3). The highest expression of *Prtb* was observed when the P19CL6 cells are beating. In P19CL6noggin cells, DMSO treatment increased the *Prtb* mRNA level, but not to the level observed in beating P19CL6 cells (Fig. 3). It is, therefore, possible that DMSO

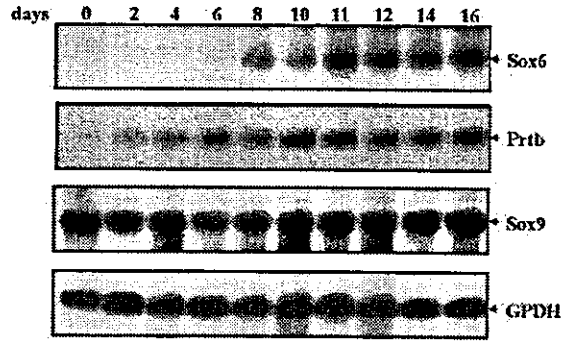

Figure 4. Northern blot analysis of *Sox6*, *Prtb* and *Sox9* expression in P19CL6 cells treated with DMSO over a time course. Each lane contains 10 μg of total RNA. Numbers above refer to days of DMSO exposure: 0 (before adding DMSO), 2, 4, 6, 8, 10, 11, 12, 14 and 16 days. The cells started to beat on day 11. Hybridization with GPDH is presented to show that the same amount of intact RNA was loaded in each lane.

treatment itself may have a partial effect on the expression of the *Prtb* gene.

The temporal expression of *Sox6* and *Prtb* in DMSO-treated P19CL6 cells was also analyzed by northern hybridization. The expression of *Sox9* was also analyzed, because Sox9 has been shown to be required for the expression of *Sox6* in chondrogenesis (21). The expression of *Sox6* was faintly detectable at day 6, with highest expression on day 11 (Fig. 4), the first day that we could see beating cells. *Prtb* was faintly detected on day 0, with highest expression on day 6 (Fig. 4). *Sox9* expression did not show any significant changes as DMSO-treated P19CL6 cells differentiated into cardiomyocytes (Fig. 4).

Regulation of L-type Ca^{2+} α_{1c} in the P19CL6 cell line

Ca^{2+} channels play a crucial role in maintaining muscle contraction in response to depolarization of the plasma membrane (22). At least five types of Ca^{2+} channels have been identified and characterized. The L-type channel is the predominant type in heart and vascular tissues. There are four subunits of the L-type Ca^{2+} channel present in the heart: α_1, α_2, δ and β, and there are also distinct isoforms of the α_1 subunit, each with a unique gene product present in various tissues. The α_{1c} subunit is expressed in cardiac and vascular smooth muscle, as well as in the brain (23). The L-type Ca^{2+} channel is critical for cardiomyocyte contraction (24). Expression of L-type Ca^{2+} α_{1c} in P19CL6 cells is dramatically down-regulated following DMSO induction to beating cardiac cells (Fig. 5). However, expression of L-type Ca^{2+} α_{1c} in P19CL6noggin cells was the same as in P19CL6 cells (with and without DMSO, data not shown).

It is possible that the expression of *Sox6* and *Prtb* may have a significant effect on the transcription of the L-type Ca^{2+} α_{1c} gene, as it has been reported that the upstream sequence of the rat L-type Ca^{2+} α_{1c} gene contains a repressor sequence between −1000 and −2000 bp relative to the transcription initiation site (25). This region contains seven consensus binding sites for Sox proteins (the potential binding sites of Prtb are unknown). We analyzed 4.1 kb of the regulatory region upstream of the L-type Ca^{2+} α_{1c} cDNA in mouse

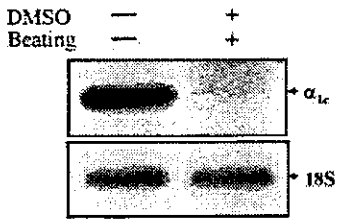

Figure 5. The L-type Ca^{2+} channel α_{1c} (α_{1c}) is down-regulated in P19CL6 cells treated with DMSO. The expression levels of the α_{1c} subunit were determined by northern blot analysis. Each lane contains 10 μg of total RNA from the cells treated as labeled (above). 18S rRNA is presented to show that the same amount of intact RNA was loaded in each lane.

(accession no. NM_009781), and detected eight perfect consensus binding sites for Sox proteins within a 1650 bp fragment located 1270 bp upstream of the published cDNA (data not shown).

To examine the direct effect of Sox6 on the expression level of L-type Ca^{2+} α_{1c}, we performed transient transfections using P19CL6 cells (Fig. 6A). We introduced *Sox6* and *Prtb* cDNA individually, or together, under the control of a CMV promoter, and analyzed the mRNA levels of the L-type Ca^{2+} α_{1c} gene by northern blot analysis. To determine the transfection efficiency, we co-transfected the cells with β-gal, driven by the CMV promoter (Fig. 6B). When transfected individually, both *Sox6* and *Prtb* down-regulated the expression of L-type Ca^{2+} α_{1c} (Fig. 6A and B). In contrast, when *Prtb* was co-transfected with *Sox6*, the expression of L-type Ca^{2+} α_{1c} remained the same as the control level.

It has been shown previously that the L-type Ca^{2+} α_{1c} transcript undergoes alternative splicing and produces three different transcripts in heart, ~15.5, 8.9 and 20 kb (26). To confirm that we were assaying gene expression and not alternative splicing, we used two different probes for L-type Ca^{2+} α_{1c} (see Materials and Methods). One probe encompassed the 5′ region of the cDNA spanning three exons and the other probe encompassed the 3′ region of the cDNA spanning four exons. We detected only the ~15.5 kb transcript in the P19CL6 and P19CL6noggin cells using either the 5′ (data not shown) or 3′ (Figs 5 and 6) probes. Thus, the different expression levels are not due to alternative splicing.

Regulation of L-type Ca^{2+} α_{1c} in p^{100H}/p^{100H} mutant mice

Next, we analyzed the expression of the L-type $Ca^{2+}\alpha_{1c}$ gene in the p^{100H}/p^{100H} mutant mouse, which is a *Sox6* null mutation that develops significant changes in the ultrastructure of cardiac and skeletal muscle, AV heart block and a cardiac conduction defect (3). RT–PCR was performed to analyze mRNA levels of the L-type $Ca^{2+}\alpha_{1c}$ gene in wild type and p^{100H}/p^{100H} hearts (Fig. 7A). Primers were selected to amplify a 548-bp fragment corresponding to nucleotides 6294–6841 of the α_{1c} subunit. Total RNA of the samples was calibrated to insure amplification in the linear range. Expression of the mouse GPDH gene was used as an internal control. In this *in vivo* assay, normal expression of *Sox6* is associated with ~1.5-fold down-regulation of the L-type Ca^{+2} α_{1c} channel (Fig. 7B), which is consistent with our *in vitro* studies (Fig. 6).

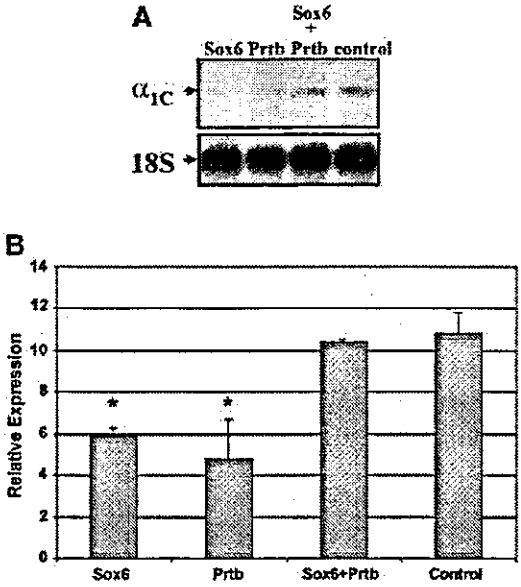

Figure 6. (A) Northern blot analysis of L-type Ca^{2+} channel α_{1c} (α_{1c}) expression in P19CL6 cells transiently transfected with *Sox6* and *Prtb* (as described in Materials and Methods). 18S rRNA is presented to show that the same amount of intact RNA was loaded in each lane. This panel shows one of three independent northern experiments. (B) The expression level values of α_{1c}, normalized for transfection efficiency by the corresponding β-Gal value. Three independent transfection experiments were done. Asterisk denotes $P \leq 0.02$ when compared with both control and co-transfection.

DISCUSSION

Sox proteins distinguish their regulatory targets in a cell type-specific fashion via co-factor binding. They recognize a motif of only 6–7 bp of DNA with considerable degeneracy. However, they appear to regulate different sets of target genes, depending on the cell type in which they are expressed. Cooperative interactions between Sox proteins and their partner factors may allow stable associations with their specific target sequences (2). To identify an interactor of the Sox6 protein we used the yeast two-hybrid system. Screening a cDNA library prepared from an embryonic day-11 mouse, we identified the *Prtb* gene (15) as an interactor with the Sox6 coiled-coil domain. The interaction was confirmed by Co-IP, demonstrating a physical interaction between the two proteins. Sequence analysis of the *Prtb* gene indicated a possible 'pair box' domain (16), suggesting that Prtb may function as a transcription factor. *Prtb* is expressed in embryonic and adult stages in multiple tissues at different levels.

P19CL6 cells provide an *in vitro* model for cardiac myocyte differentiation (11). *Sox6* is expressed exclusively when these cells are committed to differentiate to cardiac beating cells (Figs 3 and 4). *Sox6* is expressed at day 6 following DMSO induction in P19CL6 cells (Fig. 4). A minimum exposure time of 4 days of DMSO is required for differentiation of P19CL6 cells to beating myocytes (27). These findings correlate with the fact that *Sox6* is not expressed unless the cells are

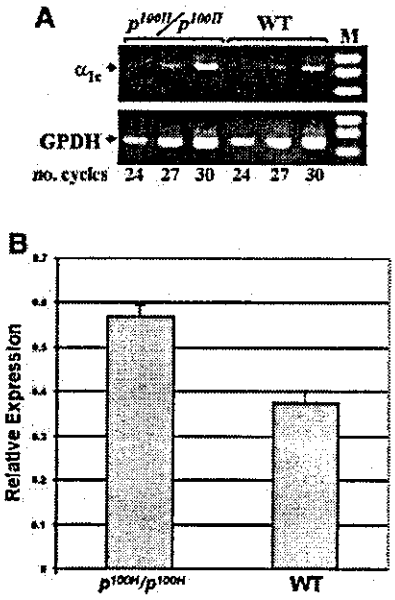

Figure 7. The expression of the L-type Ca^{2+} channel α_{1c} (α_{1c}) is up-regulated by ~1.5-fold in *Sox6* null mice (p^{100H}/p^{100H}). (A) RT–PCR products amplified from embryonic day 18.5 cardiac tissue of wild-type (WT) and p^{100H} homozygous mice (p^{100H}/p^{100H}). The numbers on the bottom indicate cycle numbers of the PCR. Sizes of the marker standards (M) are: 622, 527 and 404 bp. Amplification of the GPDH fragment was used as an internal control. (B) The amplified L-type Ca^{2+} channel α_{1c} fragment was quantified and normalized with the GPDH fragment using densitometry, and each bar represents the SD of three independent experiments.

committed to beating, with the highest expression of *Sox6* on day 11, at which point rhythmic contractions begin. The temporal expression of *Sox6* in P19CL6 cells (and the mutant phenotype p^{100H}/p^{100H} mice) suggests that Sox6 plays a significant role in cardiogenesis.

It has been shown that *Sox6*, together with L-*Sox5* and *Sox9*, undergoes up-regulation by BMP-2 during murine fracture healing (28). On the other hand, it has been shown that Sox6 is an important downstream mediator of BMP-2 signaling in chondrogenesis, whereas other signals control the expression and function of Sox9 as a chondrogenic transcription factor (8). BMPs are members of the transforming growth factor-β super family and play a crucial role in chondrogenesis as well as in cardiomyocyte differentiation (reviewed in 29). In the present study, we have shown that *Sox6* is regulated through the BMP pathway in the differentiation of cardiomyocytes (Fig. 3) using P19CL6 cells stably transfected with noggin, an antagonist of BMP (12). In addition, we have shown that *Sox9* expression was high and equal through the DMSO time course assay (Fig. 4). Thus, we suggest that Sox6 is a downstream mediator of BMP signaling in cardiogenesis as well as in chondrogenesis, and *Sox6* and *Sox9* are probably regulated differently in the cardiac system. Another study showed that *Sox9* is required for the expression of *Sox6* in chondrocyte differentiation (21). In cardiomycyte differentiation, the expression of *Sox9* may be required for the expression of *Sox6*, but it is clearly not sufficient. Hence, the inducible P19CL6 cells may make it possible to define additional factors that are upstream of *Sox6*.

Expression analysis of the *Prtb* gene in P19CL6 and P19CL6noggin cell lines showed that *Prtb* is up-regulated when the cells differentiate to beating cardiac cells. Although DMSO, by itself, has a moderate effect on the expression of this gene, its maximum expression is observed 11 days after DMSO treatment when the cardiomyocytes are beating (Figs 3 and 4). Thus, Prtb function might be specified by the cooperation of other genes such as *Sox6*.

In addition to playing a role in cardiac myocyte development, Prtb and Sox6 may also be involved in bone formation. It has been shown that *Prtb* is a serum-responsive gene in osteoblasts and is up-regulated during adhesion and possibly involved in processes such as cell cycle control and proliferation as a participant in the extracellular matrix (16). L-Sox5 and Sox6 are essential for cartilage formation (4) and are required for notochord extracellular matrix (30). Thus, it is possible that Sox6 and Prtb cooperate in bone formation.

Elucidation of the target genes of *Sox6* and *Prtb* will be important to understand the process of cardiac myocyte differentiation. The correlation between beating cardiomyocytes and *Sox6* expression allows us to evaluate proteins important in contraction as potential targets of Sox6 regulation. For example, cardiac contraction is highly dependent on the gating function of the L-type calcium channel (31). The α_{1c} subunit of the calcium channel provides the pore structure for Ca^{2+} ion entry. It has clinical relevance, since it contains the binding sites for multiple classes of drugs, collectively known as the calcium antagonists (13). To gain insights into the regulation of this channel, we analyzed its expression in P19CL6 cells. L-type Ca^{2+} α_{1c} expression in these cells is dramatically down-regulated following DMSO induction to beating cardiac cells (Fig. 5), opposite the expectation of a direct correlation between beating cells and calcium channel expression. The reduced expression of this gene might result from aberrant regulation by DMSO, as expression of L-type Ca^{2+} α_{1c} was also down-regulated in P19CL6noggin cells treated with DMSO. Another possible explanation for this reduction is that the proliferation of the cells has an impact on expression of the L-type Ca^{2+} channel. The cells beat when they grow in multilayers. In smooth muscle cells of the rat aorta it was shown that transcription of the L-type Ca^{2+} channel α_{1c} is down-regulated in the proliferative state and it is closely linked to cell growth (32). Our *in vitro* transfection data (Fig. 6A and B) suggest that the Sox6 or Prtb proteins might at least partially down-regulate the α_{1c} channel in the P19CL6 cells treated with DMSO.

The regulatory region of the L-type Ca^{2+} α_{1c} gene contains eight consensus binding sites for Sox proteins. Multiple Sox binding sites have been reported previously in several other genes regulated by Sox factors (33–35), suggesting that the L-type Ca^{2+} α_{1c} gene might be similarly regulated. Sox6 heterodimerized with Sox5, and in the presence of Sox9, cooperatively activates the expression of col2a (a chondrocyte differentiation marker) (6). On the other hand, Sox6 interacts with CtBP2 (C-terminal binding protein) and causes repression of Fgf-3 expression (36). Thus, Sox6 can function as activator or as a repressor. The transient transfection analysis showed that Sox6 and Prtb (each one by itself) down-regulated the expression level of the L-type Ca^{2+} α_{1c} channel gene

(Fig. 6A and B). However, when Sox6 and Prtb are both overexpressed, they appear to antagonize the effects of each. Prtb might antagonize Sox6 repression (or vice versa) by interacting with Sox6 and creating a complex that can no longer interact with its DNA target (37), or a Prtb-associated complex might change the chromatin structure and abrogate Sox6 function (38). It is known that Sox transcription factors bind to the minor groove of DNA causing a 70–85° bend of the DNA, consequently introducing local conformational changes (39,40). Therefore, Sox proteins may perform part of their function as architectural proteins by organizing local chromatin structure and assembling other DNA-bound transcription factors into biologically active, sterically defined, multiprotein complexes (41,42).

The p^{100H}/p^{100H} mutant mouse is a Sox6 null mutant characterized by early postnatal lethality, associated with progressive atrioventricular heart block and myopathy (3). The cardiac expression of L-type Ca^{2+} α_{1c} is up-regulated by ~1.5-fold in the p^{100H}/p^{100H} mutant mouse (Fig. 7). This *in vivo* result correlates with our cell line observations (Fig. 6). Interestingly, knockout mice for the L-type Ca^{2+} α_{1c} die before embryonic day 14.5 (43,44). Deletion of this channel leads to a selective perturbation of cardiac morphogenesis and function in early embryonic development. Further investigation will be required to understand the role of L-type Ca^{2+} α_{1c} in the arrhythmia of the *Sox6* mutant homozygote.

In conclusion, Sox6 is within the BMP pathway in the cardiac system, interacts with Prtb, and may regulate downstream genes in the heart such as the α_{1c}-subunit of the L-type Ca^{2+} channel. The inducible P19CL6 cardiac cell lines and the p^{100H}/p^{100H} mutant mice represent useful models for studying cardiac development, with important implications for understanding congenital heart disease and therapeutic intervention.

ACKNOWLEDGEMENTS

We thank our colleagues, Drs Ray Runyan, John Gardner, Ricardo Samson and Drew T. Erickson for their helpful comments on the manuscript. This work was supported by NIH grant GM43840.

REFERENCES

1. Firulli,A.B. and Olson,E.N. (1997) Modular regulation of muscle gene transcription: a mechanism for muscle cell diversity. *Trends Genet.*, **13**, 364–369.
2. Kamachi,Y., Uchikawa,M. and Kondoh,H. (2000) Pairing SOX off: with partners in the regulation of embryonic development. *Trends Genet.*, **16**, 182–187.
3. Hagiwara,N., Klewer,S.E., Samson,R.A., Erickson,D.T., Lyon,M.F. and Brilliant,M.H. (2000) *Sox6* is a candidate gene for *p100H* myopathy, heart block and sudden neonatal death. *Proc. Natl Acad. Sci. USA*, **97**, 4180–4185.
4. Smits,P., Li,P., Mandel,J., Zhang,Z., Deng,J.M., Behringer,R.R., de Crombrugghe,B. and Lefebvre,V. (2001) The transcription factors L-Sox5 and Sox6 are essential for cartilage formation. *Dev. Cell*, **1**, 277–290.
5. Connor,F., Wright,E., Denny,P., Koopman,P. and Ashworth,A. (1995) The Sry-related HMG box-containing gene Sox6 is expressed in the adult testis and developing nervous system of the mouse. *Nucleic Acids Res.*, **323**, 3365–3372.
6. Lefebvre,V., Li,P. and de Crombrugghe,B. (1998) A new long form of Sox5 (L-Sox5), Sox6 and Sox9 are coexpressed in chondrogenesis and cooperatively activate the type II collagen gene. *EMBO J.*, **17**, 5718–5733.
7. Stokes,D.G., Liu,G., Dharmavaram,R., Hawkins,D., Piera-Velazquez,S. and Jimenez,S.A. (2001) Regulation of type-II collagen gene expression during human chondrocyte de-differentiation and recovery of chondrocyte-specific phenotype in culture involves Sry-type high-mobility-group box (SOX) transcription factors. *Biochem. J.*, **360**, 461–470.
8. Fernandez-Lloris,R., Vinals,F., Lopez-Rovira,T., Harley,V., Bartrons,R., Rosa,J.L. and Ventura,F. (2003) Induction of the Sry-related factor SOX6 contributes to bone morphogenetic protein-2-induced chondroblastic differentiation of C3H10T1/2 cells. *Mol. Endocrinol.*, **17**, 1332–1343.
9. Morris,G.E. and Manilal,S. (1999) Heart to heart: from nuclearproteins to Emery–Dreifuss muscular dystrophy. *Hum. Mol. Genet.*, **8**, 1847–1851.
10. Cohen-Barak,O., Hagiwara,N., Arlt,M.F., Horton,J.P. and Briliant,M.H. (2001) Cloning, characterization and chromosome mapping of the human *SOX6* gene. *Gene*, **265**, 157–164.
11. Habara-Ohkubo,A. (1996) Differentiation of beating cardiac muscle cells from a derivative of P19 embryonal carcinoma cells. *Cell Struct. Funct.*, **21**, 101–110.
12. Monzen,K., Shiojima,I., Hiroi,Y., Kudoh,S., Oka,T., Takimoto,E., Hayashi,D., Hosoda,T., Habara-Ohkubo,A., Nakaoka,T. *et al.* (1999) Bone morphogenetic proteins induce cardiomyocyte differentiation through the mitogen-activated protein kinase kinase kinase TAK1 and cardiac transcription factors Csx/Nkx-2.5 and GATA-4. *Mol. Cell. Biol.*, **19**, 7096–7105.
13. Liu,L., O'Hara,D.S., Cala,S.E., Poornima,I., Hines,R.N. and Marsh,J.D. (2000) Developmental regulation of the L-type calcium channel α1C subunit expression in heart. *Mol. Cell. Biochem.*, **205**, 101–109.
14. Durham-Pierre,D., Gardner,J.M., Nakatsu,Y., Kink,R.A., Francke,U., Ching,A., Aquaron,R., del Marmol,V. and Brilliant,M.H. (1994) African origin of an intragenic deletion of the human P gene in tyrosinase positive oculocutaneous albinism. *Nature Genet.*, **7**, 176–179.
15. Yang,W. and Mansour,S.L. (1999) Expression and genetic analysis of prtb, a gene that encodes a highly conserved proline-rich protein expressed in the brain. *Dev. Dyn.*, **215**, 108–116.
16. Sommerfeldt,D.W., Zhi,J., Rubin,C.T. and Hadjiargyrou,M. (2002) Proline-rich transcript of the brain (prtb) is a serum-responsive gene in osteoblasts and upregulated during adhesion. *J. Cell. Biochem.*, **84**, 301–308.
17. Tell,G., Pellizzari,L. and Damante G. (1997) Transcription factor and cancer. The example of pax genes. *Adv. Clin. Path.*, **1**, 243–255.
18. Martin,G.R. (1980) Teratocarcinomas and mammalian embryogenesis. *Science*, **209**, 768–776.
19. Frasch,M. (1995) Induction of visceral and cardiac mesoderm by ectodermal Dpp in the early *Drosophila* embryo. *Nature*, **374**, 464–467.
20. Schultheiss,T.M., Burch,J.B.E. and Lassar,A.B. (1997) A role for bone morphogenetic proteins in the induction of cardiac myogenesis. *Genes Dev.*, **11**, 451–462.
21. Akiyama,H., Chaboissier,M.C., Martin,J.F., Schedl,A. and de Crombrugghe,B. (2002) The transcription factor Sox9 has essential roles in successive steps of the chondrocyte differentiation pathway and is required for expression of *Sox5* and *Sox6*. *Genes Dev.*, **16**, 2813–2828.
22. Akaike,N., Kanaide,H., Kuga,T., Nakamura,M., Sadoshima,J. and Tomoike,H. (1989) Low-voltage-activated calcium current in rat aorta smooth muscle cells in primary culture. *J. Physiol.*, **416**, 141–160.
23. Perez-Reyes,E., Wei,X.Y., Castellano,A. and Birnbaumer,L. (1990) Molecular diversity of L-type calcium channels. Evidence for alternative splicing of the transcripts of three non-allelic genes. *J. Biol. Chem.*, **265**, 20430–20436.
24. Mikami,A., Imoto,K., Tanabe,T., Niidome,T., Mori,Y., Takeshima,H., Narumiya,S. and Numa,S. (1989) Primary structure and functional expression of the cardiac dihydropyridine-sensitive calcium channel. *Nature*, **340**, 230–233.
25. Liu,L., Fan,Q.I., El-Zaru,M.R., Vanderpool,K., Hines,R.N. and Marsh,J.D. (2000) Regulation of DHP receptor expression by elements in the 5′-flanking sequence. *Am. J. Physiol. Heart Circ. Physiol.*, **278**, H1153–H1162.
26. Ma,Y., Kobrinsky,E. and Marks,A.R. (1995) Cloning and expression of a novel truncated calcium channel from non-excitable cells. *J. Biol. Chem.*, **270**, 483–493.
27. Peng,C.F., Wei,Y., Levsky,J.M., McDonald,T.V., Childs,G. and Kitsis,R.N. (2002) Microarray analysis of global changes in gene expression during cardiac myocyte differentiation. *Physiol. Genom.*, **9**, 145–155.

28. Uusitalo,H., Hiltunen,A., Ahonen,M., Gao,T.G., Lefebvre,V., Harley,V., Kahari,V.M. and Vuorio,E. (2001) Accelerated up-regulation of L-Sox5, Sox6 and Sox9 by BMP-2 gene transfer during murine fracture healing. *J. Bone Miner. Res.*, **16**, 1837–1845.
29. Monzen,K., Nagai,R. and Komuro,I. (2002) A role for bone morphogenetic protein signaling in cardiomyocyte differentiation. *Trends Cardiovasc Med.*, **12**, 263–269.
30. Smits,P., and Lefebvre,V. (2003) *Sox5* and *Sox6* are required for notochord extracellular matrix sheath formation, notochord cell survival and development of the nucleus pulposus of intervertebral discs. *Development*, **130**, 1135–1148.
31. Marsh,J.D. and Allen,P.D. (1989) Developmental regulation of cardiac calcium channels and contractile sensitivity to [Ca]o. *Am. J. Physiol.*, **256**, H179–H185.
32. Ihara,E., Hirano,K., Hirano,M., Nishimura,J., Nawata,H. and Kanaide,H. (2002) Mechanism of down-regulation of L-type Ca2+ channel in the proliferating smooth muscle cells of rat aorta. *J. Cell. Biochem.*, **87**, 242–251.
33. Peirano,R.I., Goerich,D.E., Riethmacher,D. and Wegner,M. (2000) Protein zero gene expression is regulated by the glial transcription factor Sox10. *Mol. Cell. Biol.*, **20**, 3198–3209.
34. Callard,G.V., Tchoudakova,A.V., Kishida,M. and Wood,E. (2001) Differential tissue distribution, developmental programming, estrogen regulation and promoter characteristics of cyp19 genes in teleost fish. *J. Steroid Biochem. Mol. Biol.*, **79**, 305–314.
35. Hwang,C.K., Wu,X., Wang,G., Kim,C.S. and Loh,H.H. (2003) Mouse μ opioid receptor distal promoter transcriptional regulation by SOX proteins *J. Biol. Chem.*, **278**, 3742–3750.
36. Murakami,A., Ishida,S., Thurlow,J., Revest,J.M. and Dickson,C. (2001) SOX6 binds CtBP2 to repress transcription from the *Fgf-3* promoter. *Nucleic Acids Res.*, **29**, 3347–3355.
37. Latchman,D.S. (1996) Inhibitory transcription factors. *Int. J. Biochem. Cell Biol.*, **28**, 965–974.
38. Frank,A., de-Camillis,M., Zirk,D., Chang,N., Brock,H.W. and Paro,R. (1992) Polycomb and polyhomeotic are constituents of a multimeric protein complex in chromatin of *Drosophila melanogaster*. *EMBO J.*, **11**, 2941–2950.
39. Ferrari,S., Harley,V., Pontiggia,A., Goodfellow,P.N., Lovell-Badge,R. and Bianchi,M.E. (1992) SRY, like HMG1, recognizes sharp angles in DNA. *EMBO J.*, **11**, 4497–4506.
40. Connor,F., Cary,P.D., Read,C.M., Preston,N.S., Driscoll,P.C., Denny,P., Crane-Robinson,C. and Ashworth,A. (1994) DNA binding and bending properties of the post-meiotically expressed Sry-related protein Sox-5. *Nucleic Acids Res.*, **22**, 3339–3346.
41. Werner,M.H. and Burley,S.K. (1997) Architectural transcription factors: proteins that-remodel DNA. *Cell*, **88**, 733–736.
42. Wolffe,A.P. (1994) Architectural transcription factors. *Science*, **264**, 1100–1101.
43. Seisenberger,C., Specht,V., Welling,A., Platzer,J., Pfeifer,A., Kuhbandner,S., Striessnig,J., Klugbauer,N., Feil,R. and Hofmann,F. (2000) Functional embryonic cardiomyocytes after disruption of the L-type α_{1C} (*Ca,1.2*) calcium channel gene in the mouse. *J. Biol. Chem.*, **275**, 39193–39199.
44. Klugbauer,N., Welling,A., Specht,V., Seisenberger,C. and Hofmann,F. (2002) L-type Ca2+ channels of the embryonic mouse heart. *Eur. J. Pharmacol.*, **447**, 279–284.

Circ J 2003; **67**: 1064–1067

Endoluminal Perspective Volume Rendering of Coronary Arteries Using Electron-Beam Computed Tomography

Nobusada Funabashi, MD; Kazuo Misumi, MD*; Hiroyuki Ohnishi, RT*;
Mai Watanabe, RT*; Yutaka Suzuki, RT*; Noriyuki Imai, RT*;
Katsuya Yoshida, MD; Issei Komuro, MD

Remarkable progress has been made in the treatment of coronary heart diseases because of a variety of new interventional devices, but as each new device or procedure has suitability for a particular type of patient or purpose, patient selection is increasingly important. Endoluminal perspective volume renderings of the coronary arteries of a 70-year-old male with old myocardial infarction and recurrent chest pain were carried out using electron-beam computed tomography. Conventional coronary angiography had revealed significant stenosis of the distal portion of the left anterior descending branch, and subsequent conventional balloon angioplasty had failed to expand the stenotic site. Perspective volume rendering images can distinguish differences in objects and evaluate the cross sectional area of the lumen and the morphology of calcification. In the present patient, a huge mass of calcified plaque occupied most of the lumen at a site corresponding to the angiographic site of stenosis. According to this finding, rotational atherectomy was indicated and had a good outcome. The qualitative information for characterizing and determining the morphology of atherosclerotic plaque provided by perspective volume rendering may be useful in selecting the appropriate intervention. (*Circ J* 2003; **67**: 1064–1067)

Key Words: Coronary arteries; Electron-beam computed tomography; Perspective volume rendering

Recently it has become possible to evaluate coronary arteries using non-invasive modalities such as computed tomography (CT) or magnetic resonance imaging[1,2] In addition, perspective rendering of the coronary arteries using electron-beam CT (EBCT), which has the capability of electrocardiogram triggering and has excellent temporal and spatial resolution, has been reported in conjunction with the shaded surface display technique[3] Qualitative information on the characterization and morphology of atherosclerotic plaque would be useful in selecting the appropriate device or procedure as intervention in coronary heart disease for individual patients. We report our experience with endoluminal perspective volume rendering (PVR) of the coronary arteries using EBCT.

Case Report

Both conventional coronary angiography and EBCT were performed on a 70-year-old male within a period of 24 h. He had an old myocardial infarction, and balloon angioplasty without stenting had been performed 2 years previously because of stenosis of the distal portion of the left anterior descending coronary artery (LAD). However, it had failed to expand the stenotic site and the patient had experienced recurrent chest pain for 1 month prior to this study. Conventional coronary angiograms revealed signifi-

(Received April 27, 2002; revised manuscript received June 3, 2002; accepted June 10, 2002)
*Department of Cardiovascular, Science and Medicine, Chiba University Graduate School of Medicine (M4) and *Heart Institute, Chiba-Nishi General Hospital, Chiba, Japan*
Mailing address: Issei Komuro, MD, Department of Cardiovascular Science and Medicine, Chiba University Graduate School of Medicine, 1-8-1 Inohana, Chuo-ku, Chiba City, Chiba 260-8670, Japan.
E-mail: komuro-tky@umin.ac.jp

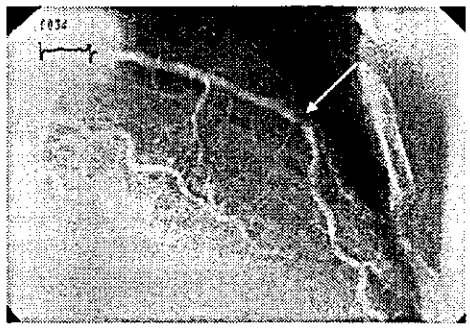

Fig 1. Conventional coronary angiogram. The right anterior oblique projection shows significant stenosis in the distal portion of the left anterior descending coronary artery (arrow).

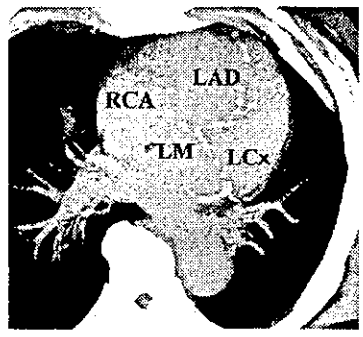

Fig 2. One thin slab maximum intensity projection image of the coronary arteries using routine electron-beam computed tomography. Much calcification is evident in the left main (LM), left anterior descending coronary artery (LAD), left circumflex branch (LCx), and right coronary arteries (RCA).

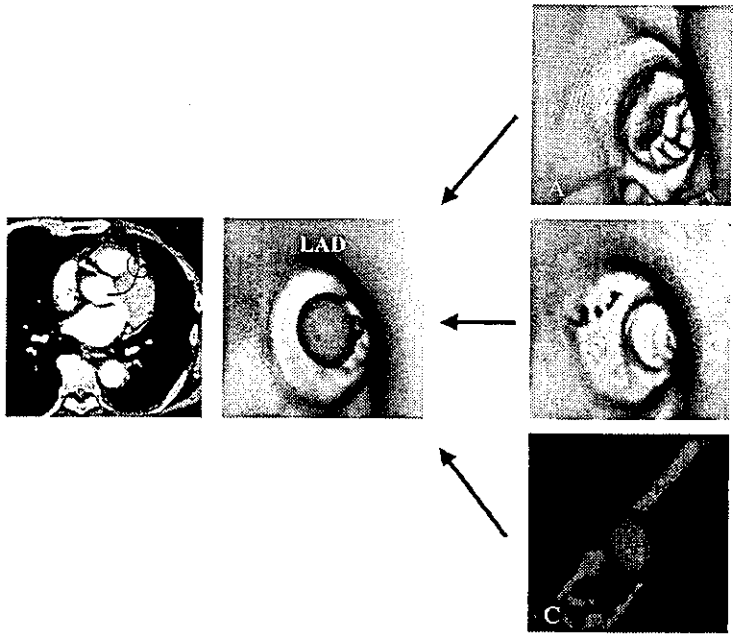

Fig3. Schema of the concept of endoluminal perspective volume rendering (PVR) images. Axial source image of enhanced electron-beam computed tomography (EBCT) and endoluminal PVR images of the coronary arteries using EBCT. The curved line and circle in the axial source image show the route of the series of endoluminal PVR images and the site of the endoluminal PVR images in (A–D), respectively. The endoluminal PVR images show the inside of the lumen of the coronary arteries. All PVR images (A–D) were of the same view and site, but with different shapes of opacity and color curves. (A) The shape of the opacity curves was set to eliminate visualization of the calcification, contrast medium from the lumen, and vessel wall, and was set to represent fatty tissue. As a result, epicardial fat was represented. The shape of the color curves was set to represent the fatty tissue as yellow. (B) The shape of the opacity curves was set to eliminate visualization of the calcifications, contrast medium from the lumen, and epicardial fat, and was set to represent the vessel wall as semitransparent. The shape of the color curves was set to represent the vessel wall as white. (C) The shape of the opacity curves was set to eliminate visualization of the contrast medium from the lumen, vessel wall and fatty tissue, and was set to represent calcified plaque with CT numbers well above those of the contrast-enhanced coronary artery lumen. The shape of the color curves was set to represent calcified plaque as red. (D) The shapes of the opacity and color curves were combined with those of A, B, and C. Epicardial fat could be observed through the semitransparent vessel wall. The form of the calcified plaque and the spatial relationship of the calcified plaque, vessel wall, and epicardial fat could be recognized.

cant stenosis of the distal portion of the LAD (Fig 1).

Next day, a routine EBCT scan (Imatron C-150XP, Imatron, South San Francisco, CA, USA) was performed to evaluate calcification of the coronary arteries. While the patient held his breath, the scan was performed in the step volume scan (SVS) mode using 3 mm collimation, 3 mm table incrementation, 100 ms scanning time and triggered to 80% of the R-to-R interval. The thin slab maximum intensity projection image indicated severe calcification on the left main, LAD, left circumflex branch, and right coronary arteries (Fig 2). Next, to evaluate the coronary arterial lumen and to make endoluminal PVR, enhanced EBCT was performed using the SVS mode with 3 mm collimation and 2 mm table incrementation and was coupled to a 150 ml intravenous injection of iodinated contrast medium (300 mgI/ml) at 2.5 ml/s with a delay time of 25 s. These data were sent to a workstation (M-900, Zio, Tokyo, Japan) and 3-dimensional (D) images were reconstructed. The endoluminal PVR images showed the inside of the lumen of the coronary arteries and we could represent the structure surrounding the lumen (vessel walls and fatty tissue) and the calcification by selecting the appropriate shape of the opacity and color curves. The shape of the opacity curves was set to eliminate visualization of the contrast medium from the lumen to show the inside of the vessel lumen, and was set as semitransparent to represent the vessel walls. Fatty tissue and calcifications were represented as completely opaque. The shape of the color curves was set to represent fatty tissue, vessel walls, and calcifications as yellow, white, and red, respectively (Fig 3). Calcified plaque with CT numbers well above those of the contrast-enhanced coronary artery lumen could be distinguished by PVR. There was a huge mass of calcified plaque occupying most of the lumen at a site approximately equal to the previously identified site of stenosis (Fig 4E,F), so high-speed rotational atherectomy of the LAD was selected as the interventional procedure and had a good result.

Discussion

EBCT obtains ultrafast scans by sweeping a steered electron beam on a fixed tungsten target ring, thereby providing a moving X-ray source without mechanical motion. The 100-ms mode is used for high-resolution cross-sectional imaging in the SVS mode with ECG gating. Therefore, EBCT is a suitable modality for cardiac imaging because of its high spatial resolution and the ability to perform ECG triggering. The spatial resolution for in-plane in EBCT is

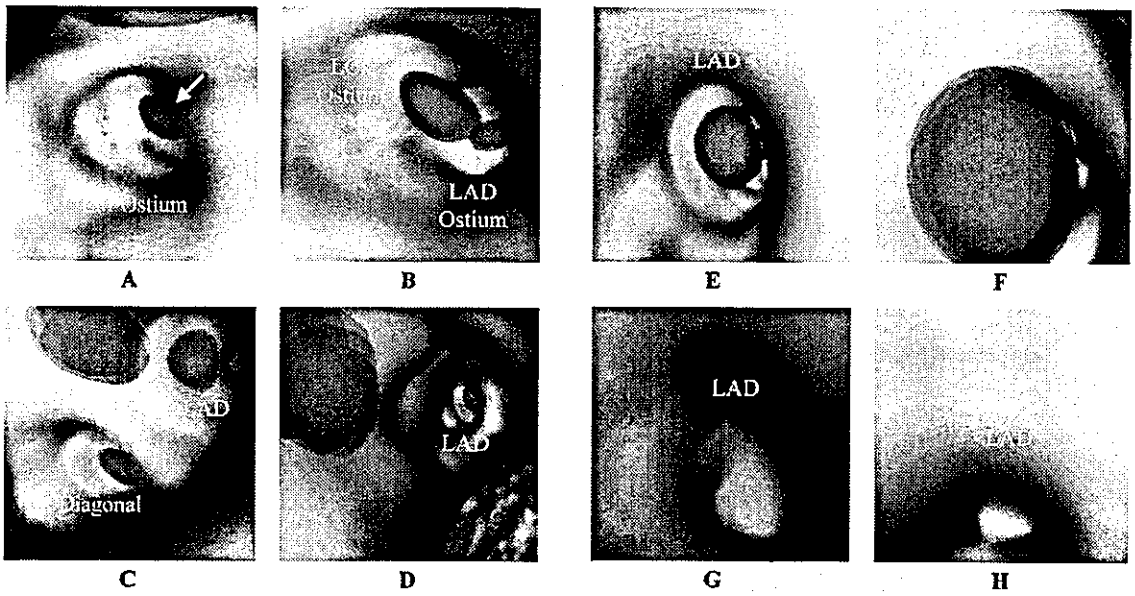

Fig4. Endoluminal perspective volume renderings of the coronary arteries using electron-beam computed tomography (EBCT) show the inside of the lumen of the coronary arteries. The shapes of the opacity curves and color curves were the same as in Fig3D. Calcified plaque with CT numbers well above those of the contrast-enhanced coronary artery lumen could be distinguished by perspective volume rendering. (A) The left main (LM) ostium is shown. Calcified plaque as represented in red is inside the LM (arrow). (B) Bifurcation of the left anterior descending coronary artery (LAD) and the left circumflex branch (LCx) is shown. Calcified plaque in the bifurcation of the LAD artery and LCx and LAD ostium can be noted. (C) Bifurcation of the LAD and the first diagonal branch (1st Diagonal) is shown. (D) The lumen of the LAD is shown. The right lower part of the vessel wall was eliminated by an inappropriate setting of the opacity curves artificially. (E,F) The lumen of the distal part of the LAD is evident. There was a huge mass of calcified plaque (arrow) and that site was approximately equal to the corresponding site of stenosis as revealed by conventional coronary angiograms. (G,H) The lumen of the further distal part of the LAD is shown. Calcified plaque was not observed, possibly because of the limits of capability of the spatial resolution of the EBCT scanner and partial volume effects.

approximately 0.71 mm.

Perspective rendering of the colon, bronchus, and aorta using helical CT data has been reported[4,5] and its advantage is that it is non-invasive compared with endoscopy and intravascular ultrasound (IVUS). In addition, the distal site can be observed by virtual passage through the stenotic site, which is difficult using real endoscopy[6] and after acquisition, the images can be reviewed from any direction desired.

With conventional angiograms and 3-D images obtained by CT and magnetic resonance angiography, the vessel lumen is observed from the outside and redundant objects, such as bone, vessels, internal organs, and muscles, must be eliminated. For coronary arteries, for example, this can take approximately 20 min even by experienced technicians; more commonly it takes approximately 1 h[7] Such time-consuming elimination of redundant objects is unnecessary with PVR because it observes the target subject from the inside as a cross sectional area.

One problem with 3-D images using CT and magnetic resonance image data is that if a fixed threshold is adopted the vessel diameter or the cross-sectional area of one part may be overestimated and those of another part underestimated because of differences in the degree of enhancement during imaging, in addition to the partial volume effect[8] Adoption of a segmented threshold using line density profile curves can provide more accurate results than the use of a fixed threshold[9] To make endoluminal PVR of coronary arteries using EBCT, we can set any threshold or opacity and color curve for each key frame to achieve a segmented threshold or opacity and color curves[3] but this methodology cannot provide information on the essential color of an atherosclerotic atheroma, such as white or yellow.

Much of the remarkable progress in the treatment of coronary heart diseases has been through advances in percutaneous transluminal coronary angioplasty, especially with regard to the variety of new interventional devices. Each new device or procedure has suitability for a particular type of patient or purpose, so patient selection is very important. Calcification is a principal factor in determining the intervention; for example, suitable sites for rotational atherectomy are those that have extensive calcification,[10] diffuse lesions, ostial lesions, or lesions that are difficult to expand.

Endoluminal PVR of coronary arteries using EBCT makes it possible to distinguish differences in objects, such as calcification, smooth muscle cells, and fatty tissue.[11] Compared with axial source images obtained by routine EBCT scanning, which has been the gold standard for detecting and quantifying coronary arterial calcification,[12] PVR images enable the clinician to evaluate the configuration of the calcification against the cross-section of the vessel lumen; for example, how closely the angle of the calcium against the lumen reaches 360° or whether the calcification is eccentric. Thus, this information, previously only available from IVUS, can be obtained non-invasively and support the selection of the appropriate intervention. A case–control study need to be performed to determine the

usefulness of PVR as a tool in selecting the appropriate intervention for coronary heart disease, and should include a comparison with the findings of IVUS.

References

1. Moshage WE, Achenbach S, Seese B, Bachmann K, Kirchgeorg M. Coronary artery stenoses: Three-dimensional imaging with electrocardiographically triggered, contrast agent-enhanced, electron beam CT. *Radiology* 1995; **196:** 707–714.
2. Shimamoto R, Suzuki J, Nishikawa J, Fujimori Y, Nakamura F, Shin WS, et al. Measuring the diameter of coronary arteries on MR angiograms using spatial profile curves. *AJR Am J Roentgenol* 1998; **170:** 889–893.
3. Nakanishi T, Kohata M, Miyasaka K, Fukuoka H, Ito K, Imazu M. Virtual endoscopy of coronary arteries using contrast-enhanced ECG triggered electron beam CT data sets. *AJR Am J Roentgenol* 2000; **174:** 1345–1347.
4. Beaulieu CF, Jefferey RB Jr, Karadi C, Paik DS, Napel S. Display modes for CT colonography: Part II. Blinded comparison of axial CT and virtual endoscopic and panoramic endoscopic volume-rendered studies 1. *Radiology* 1999; **212:** 203–212.
5. Neri E, Caramella D, Falaschi F, Sbragia P, Vignali C, Laiolo E, et al. Virtual CT intravascular endoscopy of the aorta: Pierced surface and floating shape thresholding artifacts 1. *Radiology* 1999; **212:** 276–279.
6. Rubin GD, Beaulieu CF, Argiro V, Ringl H, Norbash AM, Feller JF, et al. Perspective volume rendering of CT and MR images: Applications for endoscopic imaging. *Radiology* 1996; **199:** 321–330.
7. Achenbach S, Moshage W, Ropers D, Nossen J, Daniel WG. Value of electron-beam computed tomography for the noninvasive detection of high-grade coronary-artery stenoses and occlusions. *N Engl J Med* 1998; **339:** 1964–1971.
8. Achenbach S, Moshage W, Ropers D, Bachmann K. Comparison of vessel diameters in electron beam tomography and quantitative coronary angiography. *Int J Card Imaging* 1998; **14:** 1–7.
9. Funabashi N, Rubin GD, Kobayashi Y, Shifrin RY, Wexler L, Perlroth M. Accuracy of coronary artery dimensions with Electron-Beam CT angiography: Comparison of measurement methods. *Radiology* 1999; **213**(P): 269.
10. Brown DL, George CJ, Steenkiste AR, Cowley MJ, Leon MB, Cleman MW, et al. High-speed rotational atherectomy of human coronary stenoses: Acute and one-year outcomes from the new approaches to coronary intervention (NACI) registry. *Am J Cardiol* 1997; **80:** 60K–67K.
11. Funabashi N, Matsumoto A, Yoshida T, Watanabe S, Misumi K, Masuda Y. Usefulness of three-dimensional visualization of coronary arteries using electron-beam computed tomography data with volume rendering. *Jpn Circ J* 2000; **64:** 644–646.
12. Agatson AS, Janowitz WR, Hildner FJ, Zusmer NR Jr, Viamonte M, Detrano R. Quantification of coronary artery calcium using ultrafast computed tomography. *J Am Coll Cardiol* 1990; **15:** 827–832.